

## Article

# Hexa-Histidine, a Peptide with Versatile Applications in the Study of Amyloid- $\beta$ (1–42) Molecular Mechanisms of Action

Jairo Salazar <sup>1,\*</sup>, Alejandro K. Samhan-Arias <sup>2,3</sup>  and Carlos Gutierrez-Merino <sup>4,\*</sup> <sup>1</sup> Departamento de Química, Universidad Nacional Autónoma de Nicaragua-León, León 21000, Nicaragua<sup>2</sup> Departamento de Bioquímica, Universidad Autónoma de Madrid (UAM), C\Arzobispo Morcillo 4, 28029 Madrid, Spain; alejandro.samhan@uam.es<sup>3</sup> Instituto de Investigaciones Biomédicas 'Alberto Sols' (CSIC-UAM), C\Arturo Duperier 4, 28029 Madrid, Spain<sup>4</sup> Instituto de Biomarcadores de Patologías Moleculares, Universidad de Extremadura, 06006 Badajoz, Spain

\* Correspondence: jairochemsalazar@gmail.com (J.S.); biocgm@gmail.com (C.G.-M.)

**Abstract:** Amyloid  $\beta$  (A $\beta$ ) oligomers are the most neurotoxic forms of A $\beta$ , and A $\beta$ (1–42) is the prevalent A $\beta$  peptide found in the amyloid plaques of Alzheimer's disease patients. A $\beta$ (25–35) is the shortest peptide that retains the toxicity of A $\beta$ (1–42). A $\beta$  oligomers bind to calmodulin (CaM) and calbindin-D28k with dissociation constants in the nanomolar A $\beta$ (1–42) concentration range. A $\beta$  and histidine-rich proteins have a high affinity for transition metal ions Cu<sup>2+</sup>, Fe<sup>3+</sup> and Zn<sup>2+</sup>. In this work, we show that the fluorescence of A $\beta$ (1–42) HiLyte<sup>TM</sup>-Fluor555 can be used to monitor hexa-histidine peptide (His<sub>6</sub>) interaction with A $\beta$ (1–42). The formation of His<sub>6</sub>/A $\beta$ (1–42) complexes is also supported by docking results yielded by the MDockPeP Server. Also, we found that micromolar concentrations of His<sub>6</sub> block the increase in the fluorescence of A $\beta$ (1–42) HiLyte<sup>TM</sup>-Fluor555 produced by its interaction with the proteins CaM and calbindin-D28k. In addition, we found that the His<sub>6</sub>-tag provides a high-affinity site for the binding of A $\beta$ (1–42) and A $\beta$ (25–35) peptides to the human recombinant cytochrome *b*<sub>5</sub> reductase, and sensitizes this enzyme to inhibition by these peptides. In conclusion, our results suggest that a His<sub>6</sub>-tag could provide a valuable new tool to experimentally direct the action of neurotoxic A $\beta$  peptides toward selected cellular targets.



**Citation:** Salazar, J.; Samhan-Arias, A.K.; Gutierrez-Merino, C. Hexa-Histidine, a Peptide with Versatile Applications in the Study of Amyloid- $\beta$ (1–42) Molecular Mechanisms of Action. *Molecules* **2023**, *28*, 7138. <https://doi.org/10.3390/molecules28207138>

Academic Editor: Tibor Páli

Received: 19 September 2023

Revised: 10 October 2023

Accepted: 13 October 2023

Published: 17 October 2023



**Copyright:** © 2023 by the authors. Licensee MDPI, Basel, Switzerland. This article is an open access article distributed under the terms and conditions of the Creative Commons Attribution (CC BY) license (<https://creativecommons.org/licenses/by/4.0/>).

**Keywords:** amyloid  $\beta$ (1–42); amyloid  $\beta$ (25–35); hexa-histidine; calmodulin; calbindin-D28k; hexa-histidine-tag; recombinant cytochrome *b*<sub>5</sub> reductase; fluorescence; fluorescence resonance energy transfer

## 1. Introduction

Amyloid  $\beta$  (A $\beta$ ) peptides are a hallmark of Alzheimer's disease (AD). A $\beta$ (1–42) is the prevalent A $\beta$  peptide found in the amyloid plaques of AD patients [1]. Owing to the high affinity of A $\beta$ (1–42) for Cu<sup>2+</sup>, Fe<sup>3+</sup> and Zn<sup>2+</sup>, these metal ions are accumulated in A $\beta$  plaques [2]. Despite the fact that A $\beta$  plaques are cytotoxic, it has been proposed that A $\beta$  plaques could serve as reservoirs to assemble small A $\beta$  oligomers [3]. A $\beta$  oligomers are the main neurotoxic forms of A $\beta$  and have been linked to AD pathogenesis [4–11]. Furthermore, it has been shown that intraneuronal A $\beta$  accumulation precedes the appearance of amyloid plaques or tangles in transgenic mice models of AD [6,12–14]. A $\beta$ (25–35) is the shortest peptide that retains the toxicity of the full-length A $\beta$ (1–42) peptide [15], and it has been suggested to be the biologically active region of A $\beta$ (1–42) [16,17].

A $\beta$  peptides bind to ganglioside-clustered raft-like membrane microdomains, which foster the formation of A $\beta$  oligomers and fibrils in a cholesterol-dependent manner [18–22]. Indeed, dimeric nonfibrillar A $\beta$  has been shown to accumulate in lipid rafts in the Tg2576 mouse model of AD [23], and exogenous oligomeric A $\beta$  applied to neurons in culture concentrates in lipid rafts [24]. Moreover, plasma membrane lipid rafts play an active role in extracellular A $\beta$  uptake and internalization in neurons [25]. After the uptake of

extracellular A $\beta$ (1–42) into neurons, the intracellular aggregates elicit neuronal damage and neurotoxicity [8,9,26,27]. Intracellular targets of A $\beta$ (1–42) oligomers have been identified in the cytosol and subcellular organelles like the endoplasmic reticulum (ER) and mitochondria [28–30]. Of particular relevance are the intracellular targets of A $\beta$ (1–42) oligomers that bind nanomolar concentrations of A $\beta$  peptides, because concentrations of non-fibrillar A $\beta$  peptides within the nanomolar range have been reported in the brain [31–33], and the critical concentration that induces A $\beta$ (1–42) fibrillization lies in the submicromolar range [34,35]. Until now, dissociation constants lower than 10 nM have been reported for the complexes between A $\beta$  peptides and a few intracellular proteins expressed in brain neurons, namely calmodulin (CaM) [36], cellular prion protein [37], glycogen synthase kinase 3 $\alpha$  [38], tau [39], calbindin-D28k [40] and STIM1 [30]. However, in neurons, the concentration of CaM is in the micromolar range, which is orders of magnitude higher than the concentration of the other competing proteins in neurons listed above, with the exception of calbindin-D28k. Nevertheless, it is to be noted that, although calbindin-D28k is abundant throughout the central nervous system, including pyramidal hippocampal neurons and cortical neurons [41], the dissociation constant of the A $\beta$ (1–42)/calbindin-D28k complex is around 10-fold higher than that of the A $\beta$ (1–42)/CaM complex [40]. Due to this, CaM binds a large fraction of intracellular A $\beta$ (1–42) in the nanomolar concentration range [27].

As CaM binds A $\beta$ (1–42) and A $\beta$ (25–35) peptides with very high affinity, i.e., with a dissociation constant  $\approx$ 1 nM [36]. In a previous work, we used CaM as a template protein for the design of an antagonist peptide of A $\beta$ (1–42) using docking approaches [40]. Fluorescence assays with A $\beta$ (1–42) HiLyte<sup>TM</sup>-Fluor555 confirmed that this peptide efficiently inhibits the interaction between A $\beta$ (1–42) and CaM [40]. Interestingly, the peptide designed to bind the 25–35 amino acid residues of A $\beta$ (1–42) was experimentally found to also be a potent inhibitor of the interaction between A $\beta$ (1–42) and calbindin-D28k [40], pointing out that the same amino acid domain of A $\beta$ (1–42) is involved in its complexation with both CaM and calbindin-D28k. This bears a special relevance in AD, since these proteins play important roles in neuronal calcium signaling and the dysregulation of intracellular calcium homeostasis, and alterations of neuronal excitability have been shown to mediate A $\beta$  neurotoxicity [42–45]. On the other hand, it is known that several endogenous neuropeptides can antagonize the actions of A $\beta$ , both in animal models [46–48] and in cell cultures [49,50]. Therefore, the search for novel peptides that binds A $\beta$  with high affinity can shed light on the research of endogenous neuropeptides with neuroprotection actions against A $\beta$ . Histidine-rich proteins have a high affinity for Cu<sup>2+</sup>, Fe<sup>3+</sup> and Zn<sup>2+</sup> [51–53], like A $\beta$ (1–42) [2,54]. Thus, polyhistidine motifs or peptides are good candidates as A $\beta$ (1–42) antagonists and putative novel therapeutic agents in AD. Moreover, it has been noted that the hexa-histidine binding by monoclonal antibody C706, which recognizes the human A $\beta$  peptide, mimics A $\beta$  recognition [55].

In this work, we report that the fluorescence of A $\beta$ (1–42) HiLyte<sup>TM</sup>-Fluor555 (dye covalently bound to ASP1 of A $\beta$ ) monitors hexa-histidine peptide (His<sub>6</sub>) interaction with A $\beta$ (1–42) and the inhibition of the interaction between A $\beta$ (1–42) and the proteins CaM and calbindin-D28k. Also, we found that the presence of a C-terminal His<sub>6</sub>-tag in human recombinant cytochrome *b*<sub>5</sub> reductase (Cb5R) sensitizes its enzymatic activity to modulation by submicromolar A $\beta$ (1–42) concentrations. In this work, we have used human recombinant Cb5R because the cytochrome *b*<sub>5</sub> (Cb<sub>5</sub>)/Cb5R system has a relevant role in lipid metabolism, which is significantly altered in AD [56,57].

## 2. Results

### 2.1. Hexa-Histidine (His<sub>6</sub>) Interacts with A $\beta$ (1–42) HiLyte<sup>TM</sup>-Fluor555

The addition of submicromolar concentrations of His<sub>6</sub> to a solution of 10 nM A $\beta$ (1–42) HiLyte<sup>TM</sup>-Fluor555 increases the fluorescence intensity of the labelled peptide (Figure 1A). The kinetics of the increase in fluorescence, which monitors the interaction between His<sub>6</sub> and A $\beta$ (1–42) HiLyte<sup>TM</sup>-Fluor555, has an initial slower phase of 1–2 min and reaches a maximum of  $8 \pm 2\%$  with a half-time of approximately 10 min. Although the kinetics are

slightly faster with 0.25  $\mu\text{M}$  of His<sub>6</sub>, the large overlap between the kinetic traces obtained with 0.1 and 0.25  $\mu\text{M}$  of His<sub>6</sub> points out that at the latter concentration, no new complexes are being formed. The results of titration with His<sub>6</sub> shown in Figure 1B confirm the saturation of the maximum fluorescence change at a concentration of 0.1  $\mu\text{M}$  of His<sub>6</sub>. The small value of the maximum fluorescence change indicates that His<sub>6</sub> interaction with A $\beta$ (1–42) elicits only a small change in the microenvironment of the HiLyte<sup>TM</sup>-Fluor555 dye, which is bound to ASP1 of A $\beta$ (1–42). The short initial lag phase suggests that conformational changes in His<sub>6</sub> and/or A $\beta$ (1–42) HiLyte<sup>TM</sup>-Fluor555 are needed for a better coupling between both molecules. The dependence upon the His<sub>6</sub> concentration of the increase in fluorescence intensity at 2000 s of the kinetic of the increase in fluorescence is shown in Figure 1B. Taking into account that the noise of the fluorescence signal introduces an error close to  $\pm 2\%$  in the differences between fluorescence intensity readings, the 50% of the maximum fluorescence change is reached with a concentration of  $\approx 50$ –60 nM of His<sub>6</sub>, i.e., the saturation of the fluorescence change is observed at ratios  $\geq 10$  molecules of His<sub>6</sub> per A $\beta$ (1–42) HiLyte<sup>TM</sup>-Fluor555 monomer.

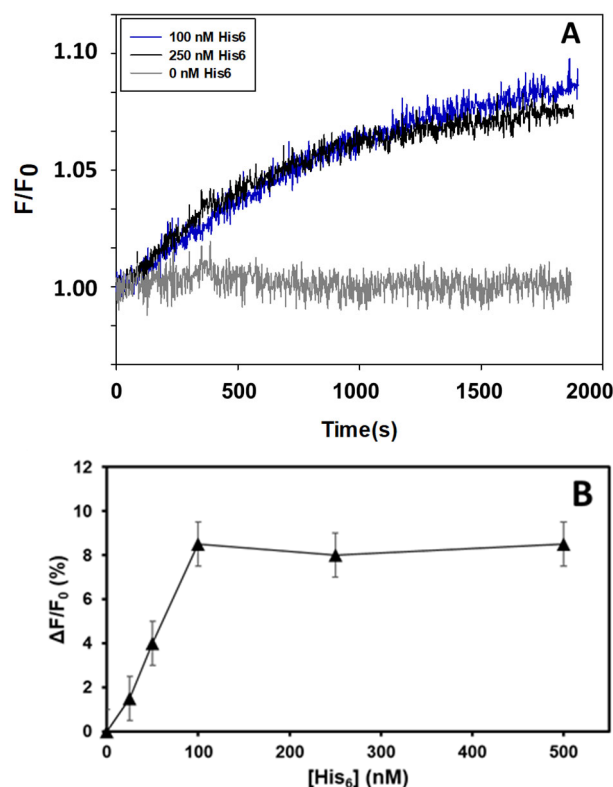


**Figure 1.** The fluorescence of A $\beta$ (1–42) HiLyte<sup>TM</sup>-Fluor555 monitors its interaction with His<sub>6</sub>. **(A)** Kinetics of the increase in A $\beta$ (1–42) HiLyte<sup>TM</sup>-Fluor555 fluorescence induced by the addition of His<sub>6</sub>. For a more direct evaluation of the magnitude of the increase in the fluorescence, the results are presented as the ratio between the fluorescence intensity at different times (F) and the fluorescence intensity at time 0 (F<sub>0</sub>). The kinetic traces shown are the means of triplicate experiments performed with 10 nM A $\beta$ (1–42) HiLyte<sup>TM</sup>-Fluor555 and the concentrations of His<sub>6</sub> indicated in the figure, which was added at time 0. The kinetic trace in gray color is the control with the addition of only the buffer in which His<sub>6</sub> is prepared (0 His<sub>6</sub>). **(B)** Dependence upon the His<sub>6</sub> concentration of the increase in the fluorescence intensity of A $\beta$ (1–42) HiLyte<sup>TM</sup>-Fluor555 at the end of the kinetic of increase in fluorescence. Other experimental conditions used for these fluorescence measurements are given in Section 4.

The experimental results shown above prompted us to perform docking between His<sub>6</sub> and/or A $\beta$ (1–42). The analysis of docking has been performed using the MDockPeP Server, as indicated in Section 4. The structure of A $\beta$ (1–42) registered with PDB ID: 1IYT in UniPro

Databank has been selected for this docking work due to the following reasons: (1) at the concentration of 10 nM used in these experiments, the A $\beta$ (1–42) peptide must be largely in the monomeric state because the dissociation constant for A $\beta$ (1–42) dimers is similar to that reported for A $\beta$ (1–40) dimers, i.e., around  $198 \pm 43$  nM [58], and (2) we found in a previous work that this structure of the A $\beta$ (1–42) monomer is a good template structure for the design of an efficient peptide antagonist for the interaction between A $\beta$ (1–42) and CaM [40]. The results generated 10 possible structural models for the complex formation, which can be grouped into three clusters, as shown in Table 1 and Supplementary Tables.

**Table 1.** Interacting interfaces for the complex formation between His<sub>6</sub> and A $\beta$  peptides obtained via molecular docking simulation.

Cluster	Involved Receptor Residues on the Interaction (A $\beta$ Peptide)	Involved Ligand Residues on the Interaction (His <sub>6</sub> Peptide)	Binding Energy $\Delta^{\ddagger}G$ (kcal/mol)
Cluster 1	LYS16, LEU1, PHE20, LA21, VAL24, GLY25, LYS2, ILE31, LEU34, MET35,	HIS1, HIS3, HIS4, HIS5, HIS6	−6.8
Cluster 2	GLU3, HIS6, ASP7, TYR10, HIS14	HIS1, HIS2, HIS6	−4.8
Cluster 3	GLY9, VAL18	HIS1, HIS2, HIS6	−2.6

In cluster 1, His<sub>6</sub> interacts with the A $\beta$ (1–42) domain close to the NH<sub>2</sub>-terminus and involves the short  $\alpha$ -helix and the part of the long  $\alpha$ -helix near the structural tilt of this peptide. Cluster 1 gathers models 1, 4, 7 and 8 and presents an estimated free energy for the complex formation of −6.8 kcal/mol, which is that found for the lowest energy model of the cluster (model 7) (Figure 2, cluster 1). The interacting interface in cluster 1 comprises the following amino acid residues of the A $\beta$  peptide: LYS16, LEU1, PHE20, ALA21, VAL24, GLY25, LYS2, ILE31, LEU34 and MET35 and HIS1, HIS3, HIS4, HIS5 and HIS6 residues of the His<sub>6</sub> peptide. Buried surface area/accessible solvent area ratio allowed us to rank those amino acid residues with higher participation in the interaction with A $\beta$  peptide: VAL24 > ALA21 > GLY25 > LEU34 > PHE20 > MET35 > LEU17 > ILE31 > LYS28 > LYS16 and a similar participation for the HIS1, HIS3, HIS4, HIS5 and HIS6 of the His<sub>6</sub> peptide. Several H-bonds and salt bridges were found in models from cluster 1 but without sharing the same amino acid residues among themselves (Supplementary Table S1).

Cluster 2 is the second most probable cluster and is representative of another four of the ten most probable outcomes generated using the MDockPeP Server. In cluster 2, His<sub>6</sub> interacts with the A $\beta$ (1–42) domain close to the COOH-terminus. Cluster 2 gathers models 2, 5, 9 and 10. Analysis with PDBePisa estimated free energy for the complex formation of −4.8 kcal/mol, which is that found for the lowest energy model of the cluster (model 9) (Figure 2, cluster 2). The interacting interface in cluster 2 comprises the following amino acid residues of the A $\beta$  peptide: GLU3, HIS6, ASP7, TYR10, HIS14 and HIS1, HIS2, HIS6 residues of the His<sub>6</sub> peptide. Buried surface area/accessible solvent area ratio allowed us to rank those amino acid residues with higher participation in the interaction with A $\beta$  peptide: TYR10 > HIS6 > GLU3 > HIS14 > ASP7 and similar participation for the HIS1, HIS2 and HIS6 of the His<sub>6</sub> peptide. Several H-bonds and salt bridges were also found in models from cluster 2, but as also accounting for cluster 1, they did not share similarities among themselves (Supplementary Table S2). A third cluster was found based on models sharing similarities in their interaction. Cluster 3 is representative of two of the ten most probable structures generated using the MDockPeP Server and predicts that His<sub>6</sub> may also interact with the long  $\alpha$ -helix part closer to the COOH-terminus of A $\beta$ (1–42). Cluster 3 gathers models 3 and 6. Analysis with PDBePisa estimated free energy for the complex formation of −2.6 kcal/mol, which is that found for the lowest energy model of the cluster (model 3) (Figure 2, cluster 3). The interacting interface in cluster 3 comprises the GLY9

and VAL184 amino acid residues of A $\beta$  peptide and HIS1, HIS2, HIS6 residues of the His<sub>6</sub> peptide. Buried surface area/ accessible solvent area ratio indicates that both amino acid residues of A $\beta$  peptide (GLY9 and VAL184) participate similarly in the interaction with the His<sub>6</sub> peptide and A $\beta$  peptide. Several H-bonds and salt bridges were also found in models from cluster 3 without sharing similarities among themselves (Supplementary Table S3).

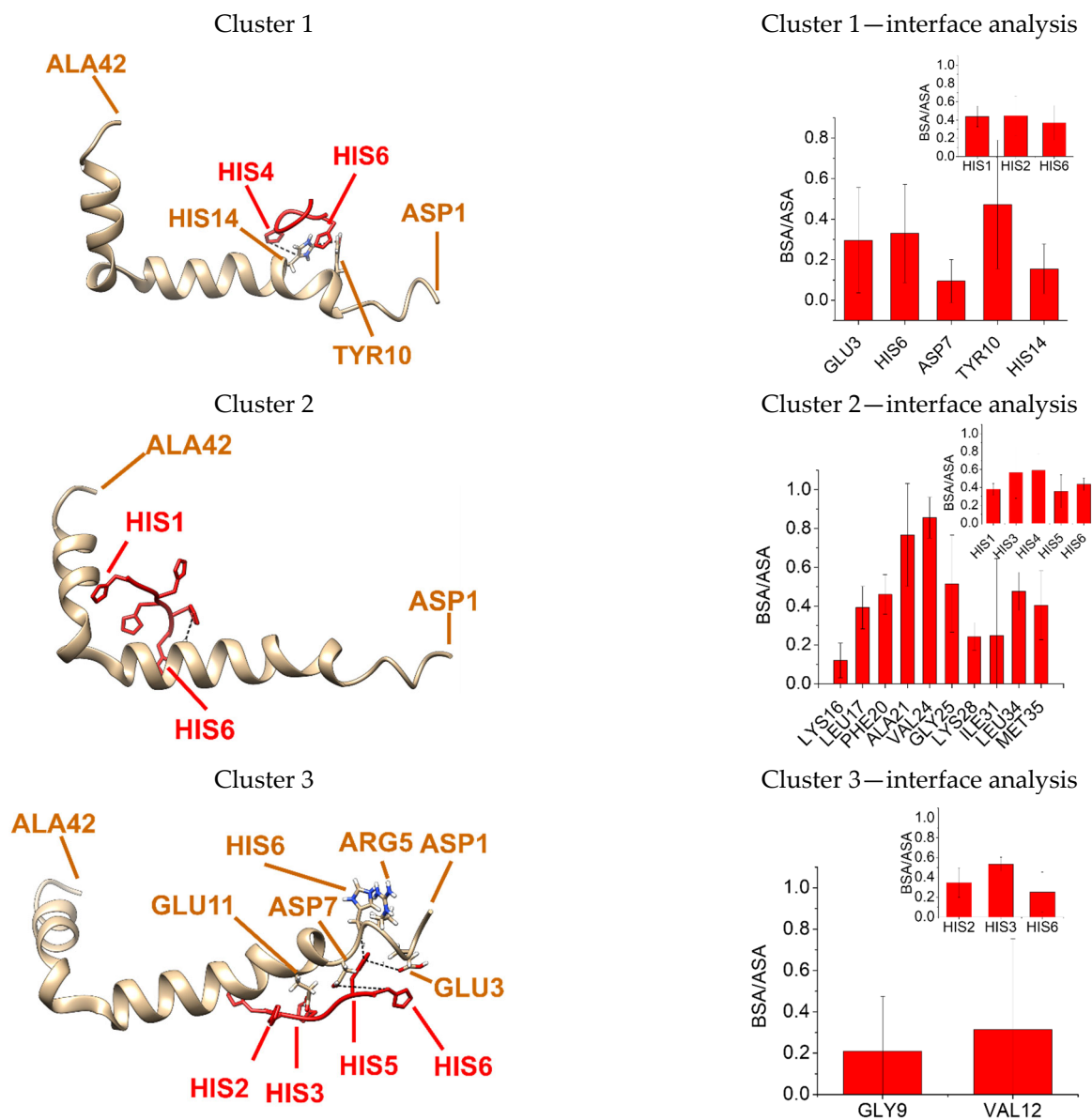


**Figure 2.** Clusters of the structures generated using the MDockPeP Server for the complex between 1His<sub>6</sub> and the structure of A $\beta$ (1–42) registered with PDB ID: 1IYT in UniPro Databank analyzed with PDBePISA. A $\beta$ (1–42) backbone is shown in brown and 1His<sub>6</sub> peptide is shown in red for the representative models with the lowest estimated binding energy of cluster1, cluster 2 and cluster 3, model 7, model 9 and model 3, respectively. H-bonds between amino acids of both structures are shown as a dotted black line.

We can summarize that the analysis *in silico* allows us to predict large conformational plasticity in the His<sub>6</sub>/A $\beta$ (1–42) complex, suggesting that the predominant conformation of this complex could be strongly affected by its microenvironment. In addition, docking results raise the possibility that the A $\beta$ (1–42) monomer can bind up to 2–3 molecules of His<sub>6</sub>.

## 2.2. His<sub>6</sub> Antagonizes the Interaction of A $\beta$ (1–42) HiLyte<sup>TM</sup>-Fluor555 with CaM and Calbindin D28k

In previous works, we have shown that A $\beta$ (1–42) binds with high affinity to CaM and calbindin-D28k [36,40]. Since model 1 predicts a strong interaction of His<sub>6</sub> with the domain of A $\beta$ (1–42) more directly involved in its interaction with CaM and calbindin-D28k, in this work, we have experimentally assessed the possibility that His<sub>6</sub> could antagonize the interaction of A $\beta$ (1–42) with these proteins.

The kinetics of the interaction of the fluorescence derivative of A $\beta$ (1–42), A $\beta$ (1–42) HiLyte<sup>TM</sup>-Fluor555, with CaM and calbindin-D28k can be monitored by the fluorescence intensity changes of the dye HiLyte<sup>TM</sup>-Fluor555 [40]. A preincubation of 15 min with His<sub>6</sub> was included in the experimental design to prevent a distortion of the kinetics of fluorescence increase produced by CaM or calbindin-D28k by the change of fluorescence elicited by His<sub>6</sub>. Figure 3 shows that His<sub>6</sub> attenuates the increase in fluorescence intensity A $\beta$ (1–42) HiLyte<sup>TM</sup>-Fluor555 after adding either calbindin-D28k or CaM. This is an effect dependent upon the concentration of His<sub>6</sub>. As shown in Figure 3, the maximum change of the fluorescence intensity and the rate of the kinetic process are decreased by His<sub>6</sub>, albeit with different efficacy. These results yield His<sub>6</sub> concentrations for a 50% attenuation of the maximum change of fluorescence intensity of  $\approx 0.1$  and  $1 \mu\text{M}$  for the interaction of A $\beta$ (1–42) with calbindin-D28k and CaM, respectively. Therefore, His<sub>6</sub> behaves as an antagonist of the interaction of A $\beta$ (1–42) with these proteins, although with different potency in the submicromolar-to-micromolar concentration range.

## 2.3. Submicromolar Concentrations of A $\beta$ Peptides Inhibit the Reduction in Cb<sub>5</sub> Catalyzed by Purified Recombinant His<sub>6</sub>-Tagged Cb5R, and No Inhibition Is Observed after Deletion of the His<sub>6</sub>-Tag

In order to evaluate the ability of His<sub>6</sub> to sensitize proteins to A $\beta$  peptides, we have used human recombinant Cb5R with a His<sub>6</sub>-tag covalently linked to the NH<sub>2</sub>-terminus amino acid, expressed and purified as described in Section 4. The NADH-dependent reduction in Cb<sub>5</sub> has been measured, following protocols used in previous works, as indicated in Section 4.

Representative kinetic traces of the rate of NADH-dependent reduction in Cb<sub>5</sub> are presented in Figure 4A. A specific activity of  $7.9 \pm 0.7 \mu\text{moles}$  of the reduced Cb<sub>5</sub>/min/mg of Cb5R at 25 °C has been calculated from initial rate measurements for the samples of human recombinant C-terminal His<sub>6</sub>-tagged Cb5R. Also, the kinetic traces shown in Figure 4A highlight the potent inhibition of this activity by nanomolar A $\beta$ (1–42) concentrations. As up to  $2 \mu\text{M}$  of A $\beta$ (1–42), the highest concentration tested in this work, we have not detected any alteration of the absorbance spectrum of Cb<sub>5</sub>, the possibility that this inhibition could be due to an A $\beta$ (1–42)-induced conformational change in the microenvironment of the heme group of Cb<sub>5</sub> can be discarded. Moreover, the inhibition is seen from the first absorbance measurements after the addition of A $\beta$ (1–42), implying its rapid binding to the inhibitory site in the Cb5R. Indeed, the observed inhibition was the same without or with up to 30 min preincubation of the Cb5R with 50 and 100 nM of A $\beta$ (1–42). Next, we removed the His<sub>6</sub>-tag from human recombinant Cb5R as described in detail in Section 4. We found that the addition of up to  $2 \mu\text{M}$  of A $\beta$ (1–42) and of A $\beta$ (25–35) does not produce a statistically significant inhibition of the rate of NADH-dependent reduction in Cb<sub>5</sub> by human recombinant Cb5R minus a His<sub>6</sub>-tag, i.e., less than 10% inhibition. Of note, a 2 micromolar concentration of A $\beta$ (1–42) oligomers is higher than those that can be expected intracellularly in AD, since the induction of fibrillization only requires submicromolar concentrations of A $\beta$ (1–42) [34,35].

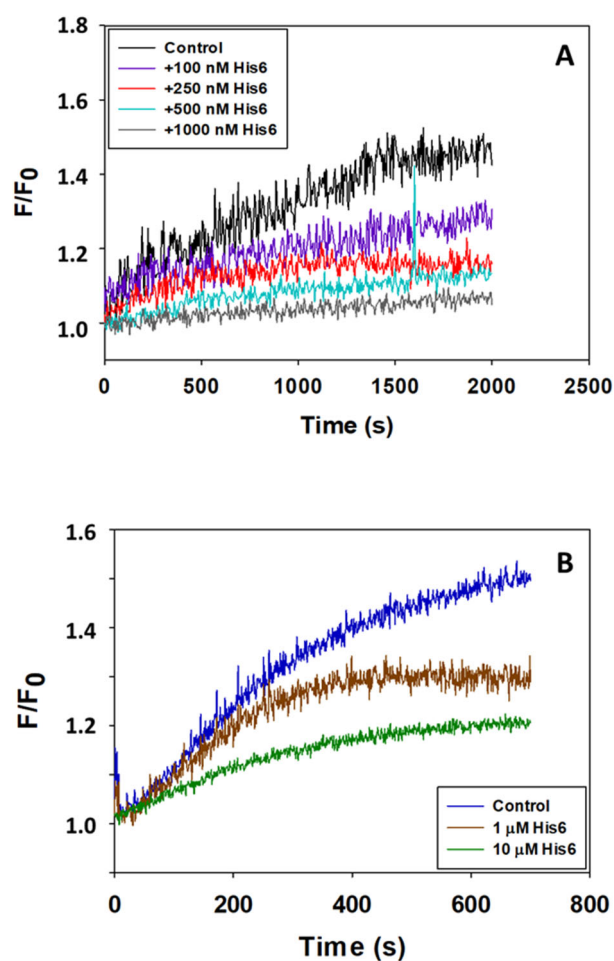


**Figure 3.** The peptide His<sub>6</sub> antagonizes the interaction of A $\beta$ (1–42) with calbindin-D28k and CaM. (A) Effect of increasing concentrations of His<sub>6</sub> on the kinetics at an increase of 10 nM A $\beta$ (1–42) HiLyte™-Fluor555 fluorescence after adding 5 nM calbindin-D28k at time 0. (B) Effect of increasing concentrations of His<sub>6</sub> on the kinetics at an increase of 10 nM A $\beta$ (1–42) HiLyte™-Fluor555 fluorescence after adding 5 nM CaM at time 0. The results are presented as the ratio between the fluorescence intensity at different times (F) and the fluorescence intensity at time 0 (F<sub>0</sub>), and the kinetic traces shown in this figure are the means of experiments performed in triplicate. The color code used for the assayed concentrations of His<sub>6</sub> is given in the inset of the figures. Other experimental conditions used for these fluorescence measurements are given in Section 4.

The results of the dependence upon the concentration of A $\beta$ (1–42) and A $\beta$ (25–35) of the inhibition of the NADH-dependent reduction in Cb<sub>5</sub> by human recombinant Cb5R with a His<sub>6</sub>-tag are shown in Figure 4B. These results showed that A $\beta$ (1–42) and A $\beta$ (25–35) are equally potent as inhibitors of this activity, without statistically significant differences between both datasets. The inhibitory effect is specific of neurotoxic A $\beta$  peptides, because a peptide with a random sequence of the 42 amino acids of A $\beta$  (scrambled A $\beta$ ), which has been found non-toxic in previous works [27,30], does not inhibit this activity (Figure 4B). The results of inhibition by A $\beta$ (1–42) and A $\beta$ (25–35) fit well to the equation for one inhibitor binding site, with an inhibition constant (K<sub>i</sub>) between 50 and 60 nM of A $\beta$  monomers, and maximum inhibition (I<sub>max</sub>) between 75 and 80%. Of note, this K<sub>i</sub> value is nearly 10-fold higher than the Cb5R concentration used in these assays, and, therefore, the contribution of the peptide bound to Cb5R to the total A $\beta$  concentration is lower than 10% at half of the saturation of the inhibition curve.

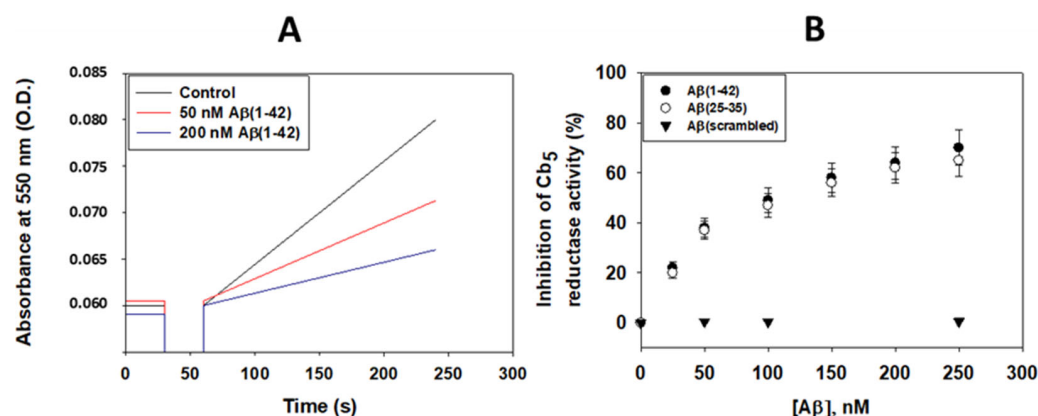


**Figure 4.** A $\beta$ (1–42) and A $\beta$ (25–35) inhibit the NADH-dependent Cb<sub>5</sub> reductase activity of the human recombinant Cb5R with a His<sub>6</sub>-tag. (A) Kinetics of Cb<sub>5</sub> reduction by the human recombinant Cb5R with a His<sub>6</sub>-tag in the absence and presence of 50 and 100 nM A $\beta$ (1–42). (B) Dependence upon the concentration of A $\beta$ (1–42), A $\beta$ (25–35) and scrambled A $\beta$ (1–42) of the inhibition of the Cb<sub>5</sub> reductase activity of the human recombinant Cb5R with a His<sub>6</sub>-tag. The results shown are the means  $\pm$  standard error of the mean (S.E.M.) of experiments performed in triplicate. Other experimental conditions used for these assays are given in the Section 4.7.

Combining these kinetic results, it merges the conclusion that the Cb<sub>5</sub> reductase activity of the His<sub>6</sub>-tagged Cb5R is strongly sensitized to neurotoxic A $\beta$  peptides.

#### 2.4. The Binding of A $\beta$ (1–42) and of A $\beta$ (25–35) to the Human Recombinant Cb5R with a His<sub>6</sub>-tag Increases the Fluorescence of Its Prosthetic Group FAD

In previous works [59,60], we have shown that the fluorescence of the prosthetic group FAD can be used to monitor conformational changes of Cb5R, which impair its catalytic activity.

In this work, we found that the addition of A $\beta$ (1–42) and of A $\beta$ (25–35) produces an increase in the FAD fluorescence of human recombinant Cb5R with a His<sub>6</sub>-tag without a significant shift of the emission peak wavelength due to a conformational change that leads to an increase in the quantum yield of FAD bound to the Cb5R. Figure 5 shows that the FAD fluorescence increase depends on the concentration of the A $\beta$ (1–42) and of A $\beta$ (25–35) peptides. Moreover, both the magnitude and the dependence upon the A $\beta$  peptide concentration of the change of FAD fluorescence are not significantly different between A $\beta$ (1–42) and A $\beta$ (25–35). Of note, this is an effect produced by the assayed neurotoxic peptides because up to 1  $\mu$ M of “scrambled” A $\beta$ (1–42) peptide does not elicit a statistically significant change in FAD fluorescence. The results obtained for the dependence of the increase in FAD fluorescence upon the concentration of A $\beta$ (1–42) and of A $\beta$ (25–35) fit well into the equation for one-site ligand–protein interaction (Figure 5). The non-linear fit of the results to this equation yields an increase of  $41 \pm 4\%$  of the FAD fluorescence at saturation with these peptides, and an A $\beta$  concentration for 50% of the effect of  $75 \pm 5$  nM of peptide monomer. Since the concentration of Cb5R in the fluorescence assays is  $32 \pm 3$  nM, the real free-peptide concentration at 50% saturation allows us to calculate an apparent dissociation constant ( $K_{d,app}$ ) of  $59 \pm 5$  nM for the complex between the Cb5R and the A $\beta$  peptide. This  $K_{d,app}$  value is within the range of values obtained for the  $K_i$ , pointing out that the binding of the A $\beta$  peptide to this site causes the inhibition of the NADH-dependent Cb<sub>5</sub> reductase activity of the human recombinant Cb5R with a His<sub>6</sub>-tag. Since the dependence of the FAD fluorescence upon the concentration of A $\beta$ (1–42) was the same in the absence and presence of 5  $\mu$ M of Cb<sub>5</sub>, the possibility that A $\beta$  could interact with the Cb<sub>5</sub> binding domain in the Cb5R can be excluded. Also, this result indicates that A $\beta$ (1–42) does not bind to Cb<sub>5</sub>, resulting in further experimental support to our conclusion derived from the lack of effect of A $\beta$ (1–42) on the absorbance spectrum of Cb<sub>5</sub> (see above).

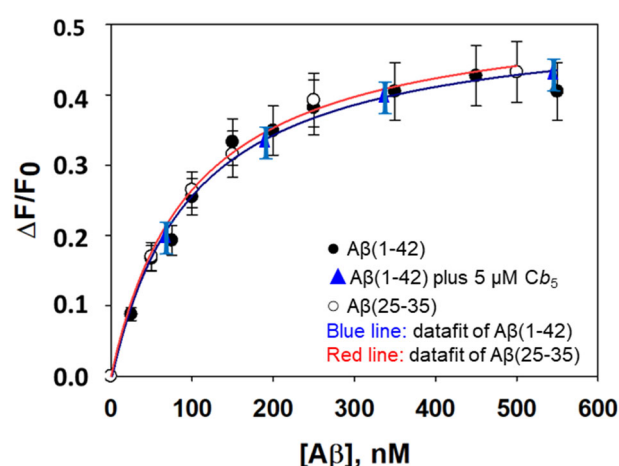


**Figure 5.** Dependence upon the concentration of A $\beta$ (1–42) and A $\beta$ (25–35) of the increase in FAD fluorescence ( $\Delta F/F_0$ ) bound to the human recombinant Cb5R with a His<sub>6</sub>-tag. There was not a significant difference between the titration of FAD fluorescence with A $\beta$ (1–42) in the absence (filled black circles) and the presence of 5  $\mu$ M Cb<sub>5</sub> (blue triangles). The lines are the results obtained via non-linear regression fit to the equation for 1:1 ligand binding site per protein molecule. The fit of the data yielded the following results:  $Y = -0.0095 + [0.5227 \times x / (96.92 + x)]$  ( $R^2 = 0.9870$ ) for A $\beta$ (1–42), and  $Y = -0.0019 + [0.5311 \times x / (99.253 + x)]$  ( $R^2 = 0.9974$ ) for A $\beta$ (25–35). The results shown are the means  $\pm$  S.E.M. of experiments performed in triplicate. Other experimental conditions used for these fluorescence measurements are given in Section 4.

In order to further assess the interaction between A $\beta$ (1–42) and human recombinant Cb5R with a His<sub>6</sub>-tag, we have used the fluorescent derivative A $\beta$ (1–42) HiLyte<sup>TM</sup>-Fluor555. This compound can act as a fluorescence resonance energy transfer (FRET) acceptor of FAD fluorescence as illustrated by the overlap between the emission fluorescence spectrum of FAD and the absorbance spectrum (Figure 6A). Next, we calculated the distance for 50% FRET efficiency ( $R_0$ ) between FAD and A $\beta$ (1–42) HiLyte<sup>TM</sup>-Fluor555 as described in Section 4, following a protocol used in previous works [61–63]. A value of  $3.96 \times 10^{-3}$  has been calculated for the quantum yield of FAD bound to the Cb5R ( $\Phi_D$ ), using as reference the quantum yield of FMN given in standard fluorescence data tables. A value of the overlap integral  $J(\lambda)$  of  $6.0254174 \times 10^{15} \text{ cm}^3 \cdot \text{M}^{-1}$  has been calculated from the recorded emission spectrum of FAD bound to the Cb5R and the absorbance spectrum of A $\beta$ (1–42) HiLyte<sup>TM</sup>-Fluor555. An  $R_0$  value of 2.77 nm has been obtained by applying the equation given in Section 4, assuming a random orientation between donor and acceptor.

Then, we recorded the emission spectrum of human recombinant Cb5R with a His<sub>6</sub>-tag in the absence and presence of 100 nM of A $\beta$ (1–42) HiLyte<sup>TM</sup>-Fluor555 and the emission spectrum of 100 nM A $\beta$ (1–42) HiLyte<sup>TM</sup>-Fluor555 in the absence of Cb5R (Figure 6B). Next, the latter spectrum, which is due to the direct excitation of the acceptor HiLyte-Fluor555, has been subtracted to the emission spectrum of Cb5R plus 100 nM of A $\beta$ (1–42) HiLyte<sup>TM</sup>-Fluor555, and the result is shown in Figure 6C. We avoided the use of a saturating concentration of the A $\beta$ (1–42)-induced increase in the FAD fluorescence in Cb5R shown in Figure 5 to prevent the complications of analysis coming from an excessively large peak of the HiLyte<sup>TM</sup>-Fluor555 fluorescence on the overall emission spectrum. The results shown in Figure 6C indicate that 100 nM of A $\beta$ (1–42) HiLyte<sup>TM</sup>-Fluor555 produces a  $45 \pm 5\%$  quenching of the peak donor FAD fluorescence at 525 nm, and a similar increase in the peak of the acceptor HiLyte<sup>TM</sup>-Fluor555 fluorescence at 555 nm. Thus, FRET measurements provide an additional proof of interaction between Cb5R with a His<sub>6</sub>-tag and A $\beta$ (1–42) HiLyte<sup>TM</sup>-Fluor555.

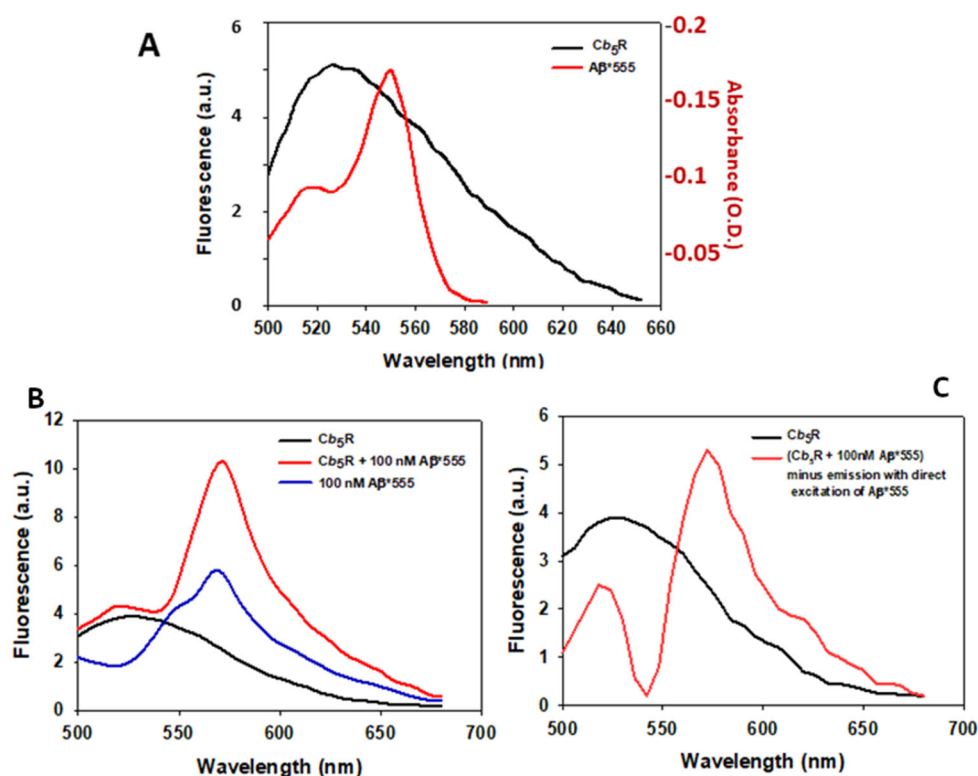


**Figure 6.** FRET between FAD bound to the human recombinant Cb5R with a His<sub>6</sub>-tag and Aβ(1–42) HiLyte™-Fluor555. (A) Emission spectrum of the human recombinant Cb5R with a His<sub>6</sub>-tag with an excitation wavelength of 460 nm (black line) and absorption spectrum of Aβ(1–42) HiLyte™-Fluor555 (Aβ\*555, red line). (B) Emission spectra of the human recombinant Cb5R with a His<sub>6</sub>-tag in the absence (black line) and presence of 100 nM of Aβ(1–42) HiLyte™-Fluor555 (Aβ\*555) (red line), and of 100 nM Aβ(1–42) HiLyte™-Fluor555 in the absence of Cb5R (direct excitation spectrum, blue line). Excitation wavelength = 460 nm, excitation and emission slits = 10 nm. (C) Emission spectrum of the human recombinant Cb5R with a His<sub>6</sub>-tag (black line) and the result of the emission spectrum of (Cb5R plus 100 nM of Aβ(1–42) HiLyte™-Fluor555) after the subtraction of the emission spectrum of 100 nM Aβ(1–42) HiLyte™-Fluor555 in the absence of Cb5R (red line). Other experimental conditions used for these fluorescence measurements are given in Section 4.

### 3. Discussion

The results show the interaction between Aβ(1–42) HiLyte™-Fluor555 and submicromolar concentrations of His<sub>6</sub>. Likely, this interaction will be further potentiated by transition metal ions, which bind with very high affinity to Aβ(1–42) [2,54], and, also, to His<sub>6</sub> [64]. Indeed, we cannot completely exclude that trace amounts of transition metal ions, which are present in the preparations of commercial samples of Aβ peptides and in buffers, are playing a role in the Aβ(1–42) HiLyte™-Fluor555/His<sub>6</sub> complexes formed under our experimental conditions. The kinetics of the increase in Aβ(1–42) HiLyte™-Fluor555 fluorescence intensity after the addition of His<sub>6</sub> is a relatively slow process for this type of molecules, with a half-time of around 10 min, and an initial short lag phase within the first minute. Therefore, the kinetic results suggest the occurrence of conformational changes in the formation of a complex between Aβ(1–42) HiLyte™-Fluor555 and His<sub>6</sub>. Also, it is to be noted that a concentration of 100 nM His<sub>6</sub> is almost saturating for its complexation with 10 nM Aβ(1–42) HiLyte™-Fluor555, indicating that the dissociation constant (K<sub>d</sub>) of this complex is in the submicromolar concentration range. However, the maximum increase in the Aβ(1–42) HiLyte™-Fluor555 fluorescence intensity (<10%) is not large enough over the noise of the data to obtain a reliable K<sub>d</sub> value for this complex from the dependence upon the His<sub>6</sub> concentration using this experimental approach.

Docking simulations provide a rational support for the formation of a complex between His<sub>6</sub> and Aβ(1–42). The simulations performed using the CABS-dock Web Server, which do not require the input of an initial conformation of His<sub>6</sub>, yield three-dimensional structures for this complex that can be grouped in three-classes taking into account the Aβ(1–42) peptide domain directly interacting with His<sub>6</sub>. Thus, changes in the structure of His<sub>6</sub> are one likely cause of the short initial lag phase of the kinetics of complex formation. On the other hand, the cluster of poses represented by cluster 1 of Figure 2, generated using docking simulations for the His<sub>6</sub>/Aβ(1–42) complex, predicts that His<sub>6</sub> interacts with amino acid residues 24–42 of Aβ(1–42). In a previous work [40], we have shown that this domain of Aβ(1–42) is the most directly involved in the formation of Aβ(1–42)/CaM and Aβ(1–42)/calbindin-D28k complexes. However, docking analysis predicts a relevant contribution of LYS28 and LYS16 in the case of the cluster 1 of the His<sub>6</sub>/Aβ(1–42) complex, the first cluster ranked by energy calculations, while only highly hydrophobic amino acids of Aβ(1–42) are involved in the interaction interface with CaM and calbindin-D28k [40]. The contribution of electrostatic interactions and H-bonds in the interface of interaction between His<sub>6</sub> and Aβ(1–42) is even stronger in the structures of the cluster 2 of His<sub>6</sub>/Aβ(1–42) complex, the second ranked by free energy calculations, as the buried surface area/ accessible solvent area ratio results in the following amino acid residues with higher participation in the interaction with the Aβ peptide: TYR10 > HIS6 > GLU3 > HIS14 > ASP7. Also, the presence of charged amino acids ASP1, GLU3, ARG5, ASP7 and GLU11 in the Aβ(1–42) domain of the interacting interface of cluster 3 of His<sub>6</sub>/Aβ(1–42) complex lends further support to the higher relevance of electrostatic interactions in the formation of this complex. Thus, docking analysis points out a higher contribution of electrostatic interactions and H-bonds in the His<sub>6</sub>/Aβ(1–42) complex than in Aβ(1–42)/CaM and Aβ(1–42)/calbindin-D28k complexes. Consistent with this analysis, in this work, we show that His<sub>6</sub> efficiently antagonizes the interaction between Aβ(1–42) HiLyte<sup>TM</sup>-Fluor555 and these two proteins, with concentrations for 50% effect ≤1 μM of His<sub>6</sub>, values that are more than 10-fold higher than those obtained for the hydrophobic peptide VFAFAMAFML(amidated-C-terminus amino acid) in our previous work [40]. However, it is to be noted that the dye HiLyte<sup>TM</sup>-Fluor555 is covalently bound to the NH<sub>2</sub>-terminus amino acid of Aβ(1–42), which is distant from the amino acid residues 24–42 of Aβ(1–42). Since fluorescence measurements point out that the interaction of His<sub>6</sub> with Aβ(1–42) HiLyte<sup>TM</sup>-Fluor555 alters the microenvironment of HiLyte<sup>TM</sup>-Fluor555, it is likely that the structure of the His<sub>6</sub>/Aβ(1–42) complex can be better described by a weighted combination of the three different clusters of His<sub>6</sub>/Aβ(1–42) complex shown in Figure 2 or that the molecular stoichiometry of this complex is higher than 1:1. Indeed, the cluster 2 in Figure 2, the second most probable model yielded by docking simulations, predicts the binding of His<sub>6</sub> to the NH<sub>2</sub>-terminus domain of Aβ(1–42). Nevertheless, the possibility of a significant generation of 3His<sub>6</sub>/Aβ(1–42) complex is unlikely because of the large difference in free energies between clusters 1 and 3, and, also, because of steric hindrance between the His<sub>6</sub> position in clusters 2 and 3. In addition, a shift between cluster structures during the formation of the His<sub>6</sub>/Aβ(1–42) complex could provide a simple explanation for the slow kinetics of interaction between His<sub>6</sub> and Aβ(1–42) HiLyte<sup>TM</sup>-Fluor555. This is a plausible possibility because docking simulations do not yield large differences of the free energy changes predicted for the clusters 1 and 2 of the His<sub>6</sub>/Aβ(1–42) complex. Further extensive experimental studies will be required to obtain the molecular stoichiometry and structure of the His<sub>6</sub>/Aβ(1–42) complex with atomic resolution.

The high affinity of His<sub>6</sub> for neurotoxic Aβ peptides, like Aβ(1–42) and Aβ(25–35), is further demonstrated by the results obtained in this work with human recombinant Cb5R with a His<sub>6</sub>-tag. First, the inhibition of the Cb<sub>5</sub> reductase activity of human recombinant Cb5R with a His<sub>6</sub>-tag by Aβ(1–42) or Aβ(25–35) has a K<sub>i</sub> of 50–60 nM of Aβ peptide monomers, while up to 2 μM of Aβ(1–42) monomers produce less than 10% inhibition of this activity of Cb5R after removal of the His<sub>6</sub>-tag. Second, this K<sub>i</sub> value is not significantly different from the value of the apparent dissociation constant of the complex between

A $\beta$ (1–42) or A $\beta$ (25–35) and human recombinant Cb5R with a His<sub>6</sub>-tag calculated from titrations with these A $\beta$  peptides of the fluorescence of FAD, the prosthetic group of this enzyme. Since the predominant aggregation state of the A $\beta$ (1–42) solutions used in our experimental conditions is the dimer, see Section 4, our results yield values  $\leq 30$  nM of A $\beta$ (1–42) dimers for both  $K_i$  and  $K_{d,app}$ . Thus, we conclude in this work that the His<sub>6</sub>-tag strongly potentiates the binding of the neurotoxic peptides A $\beta$ (1–42) and A $\beta$ (25–35) to the human recombinant Cb5R. In addition, our results point out that the Cb<sub>5</sub> reductase activity of the human recombinant Cb5R minus the His<sub>6</sub>-tag is not significantly inhibited by up to 2  $\mu$ M of A $\beta$ (1–42) oligomers, an intracellular concentration that is unlikely to be reached within the cells because the critical concentration for the induction of A $\beta$ (1–42) fibrillization is in the submicromolar range [34,35]. Of note, a ‘scrambled’ non-toxic A $\beta$ (1–42) peptide used in previous works [27,30] does not bind to the His<sub>6</sub>-tag of the human recombinant Cb5R, nor produces a significant inhibition of its activity. As the insertion of a His<sub>6</sub>-tag is widely used to help with the purification of recombinant proteins, this conclusion strongly suggests removing it prior to using these recombinant proteins in studies dealing with the biochemical and biological effects of A $\beta$ (1–42).

The large increase in the intensity of the fluorescence of its prosthetic group FAD monitors the binding of A $\beta$ (1–42) and A $\beta$ (25–35) to human recombinant Cb5R with a His<sub>6</sub>-tag. Since the catalytic site does not overlap with the position of the His<sub>6</sub>-tag bound to the NH<sub>2</sub>-terminus amino acid of Cb5R, the inhibition by A $\beta$ (1–42) or A $\beta$ (25–35) of its Cb<sub>5</sub> reductase activity is due to a long-distance induced conformational change. Taking into account that 100 nM of A $\beta$ (1–42) HiLyte<sup>TM</sup>-Fluor555 lies between 60 and 65% of the saturating concentration of Cb5R (Figure 5), we can calculate that at a saturation by A $\beta$ (1–42) HiLyte<sup>TM</sup>-Fluor555, the quenching of the donor FAD fluorescence will rise up to  $70 \pm 7\%$ . As at this concentration of A $\beta$ (1–42), the peptide will be in equilibrium between monomers and dimers [58], we have calculated the most probable distance range between FAD and the dye HiLyte<sup>TM</sup>-Fluor555 using the equation for FRET for 1 and 2 acceptors per donor with the assumption of random orientation given in Section 4. The upper distance limit of this range will be set by the case of the two acceptors HiLyte<sup>TM</sup>-Fluor555 dyes, one bound to each monomer, located equidistant from the donor FAD. The calculated distances between the donor FAD group of Cb5R and the acceptor HiLyte<sup>TM</sup>-Fluor555 dye covalently linked to A $\beta$ (1–42) have been 2.35 nm and 3.1 nm for 1 or 2 equidistant acceptors, respectively. Of note, the measurements of the anisotropy of the FAD fluorescence, performed as indicated in Section 4, presented anisotropy values lower than 0.005. As noted in [65], with this low value of donor anisotropy, there is >90% probability that the above-calculated distance range is correct. In order to evaluate whether the structural coupling between the known structures of the Cb5R and A $\beta$ (1–42) allows for the satisfaction of this requirement, we have performed docking between the soluble human erythrocytes isoform of Cb5R (PDB ID: 1UMK) and A $\beta$ (1–42) (PDB ID: 1IYT) using the ClusPro Web Server as described in Section 4. Among the 10 model structures generated in silico, we selected the model structure of the complex between Cb5R and A $\beta$ (1–42) shown in Figure 7, in which the A $\beta$ (1–42) lies close to the His<sub>6</sub>-tag bound to the NH<sub>2</sub>-terminus amino acid of the human recombinant Cb5R. This model structure satisfies the above distance requirement between the NH<sub>2</sub>-terminus amino acid of the A $\beta$ (1–42) and FAD derived from FRET measurements, which can be estimated between 2 and 3 nm by taking into account the uncertainty of the orientation and size of the HiLyte<sup>TM</sup>-Fluor555 dye in the complex. In addition, this model structure shows that the amino acids 25–35 of the A $\beta$ (1–42) lies near the catalytic center, where the isoalloxazine ring of the FAD prosthetic group of the Cb5R is located. Also, the Cb<sub>5</sub> binding site in the Cb5R, identified in previous works [66,67], lies close to the FAD group in the protein domain located as shown below in Figure 7. The extensive overlap of the 25–35 amino acid residues of the A $\beta$ (1–42) with the Cb<sub>5</sub> domain suggests that steric hindrance and/or an incorrect orientation of bound Cb<sub>5</sub> could account for the inhibition of the Cb<sub>5</sub> reductase activity measured in this work.

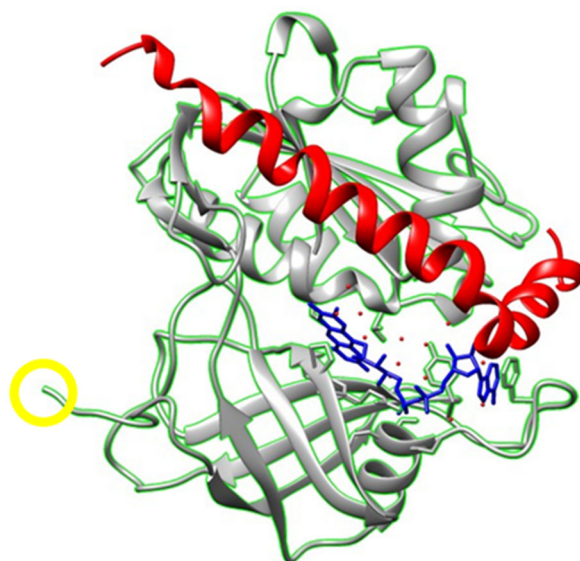


**Figure 7.** Simulation generated using docking between the soluble human erythrocytes isoform of Cb5R (PDB ID: 1UMK) and Aβ(1–42) (PDB ID: 1IYT) using the ClusPro Web Server. The polypeptide backbone of Cb5R is shown in gray/green, with the position of the prosthetic group FAD in blue, and the Aβ(1–42) is shown in red. The NH<sub>2</sub>-terminus amino acid of the Cb5R is labeled with a yellow circle.

In summary, His<sub>6</sub> binds with high affinity to Aβ(1–42), and at micromolar concentrations antagonizes the formation of Aβ(1–42)/CaM and Aβ(1–42)/calbindin-D28k complexes. In addition, a His<sub>6</sub>-tag provides a high-affinity site for the binding of neurotoxic Aβ(1–42) and Aβ(25–35) peptides to the human recombinant Cb5R, and sensitizes this enzyme to inhibition by these peptides. Therefore, our results suggest that a His<sub>6</sub>-tag could be used to experimentally direct the action of neurotoxic Aβ peptides toward selected cellular targets.

#### 4. Materials and Methods

##### 4.1. Chemicals

Human Aβ(1–42)-HiLyte<sup>TM</sup>-Fluor555 was purchased from AnaSpec (Freemont, CA, USA). Aβ(1–42), Aβ(25–35) and Aβ ‘scrambled’ were supplied by StabVida (Caparica, Portugal) and GenicBio Limited (Shanghai, China). His<sub>6</sub> was purchased from Quimigen (Madrid, Spain). Bovine brain CaM and Thrombin Clean Cleavage<sup>TM</sup> kit were purchased from Merck-Sigma-Aldrich (Madrid, Spain).

All the other chemicals used in this work were of analytical grade and supplied by Merck-Sigma-Aldrich (Madrid, Spain) and ThermoFisher Scientific (Madrid, Spain).

##### 4.2. Preparation of Aβ(1–42) Solutions

Stock Aβ(1–42) solutions were prepared by dissolving the lyophilized peptide at 4 mg/mL in 1% NH<sub>4</sub>OH. Later, the stock Aβ(1–42) solution was diluted in phosphate-buffered saline to a concentration of 177 μM. The aggregation state of Aβ(1–42) in the 177 μM solution has been assessed in Tricine–sodium dodecyl sulfate–polyacrylamide gel electrophoresis (SDS-PAGE) as described in our previous works [27,40]. As shown in [27,40], in this solution, dimers account for approximately 90% of Aβ(1–42) and trimers for ≤10%, while monomers and higher molecular species are almost undetectable.

##### 4.3. Preparation of the Human Recombinant Cb5R Soluble Isoform

Clones of the soluble isoform of human Cb5R prepared in a previous work were used to express and purify the recombinant protein purified as indicated in [67]. The purified protein was aliquoted and conserved in 30% glycerol at –80 °C until use.

The C-terminal His<sub>6</sub>-tag recombinant Cb5R has a thrombin-cutting site between the His<sub>6</sub>-tag and the enzyme, as previously shown [67]. The His<sub>6</sub>-tag was cut by overnight incubation at 4 °C with the Thrombin Clean Cleavage™ kit. The recombinant Cb5R minus the His<sub>6</sub>-tag was separated from the cleaved peptide via column chromatography through Sephadex G75 (1 × 25 cm), and the efficient removal of the His<sub>6</sub>-tag was confirmed using SDS-PAGE (Figure 8).

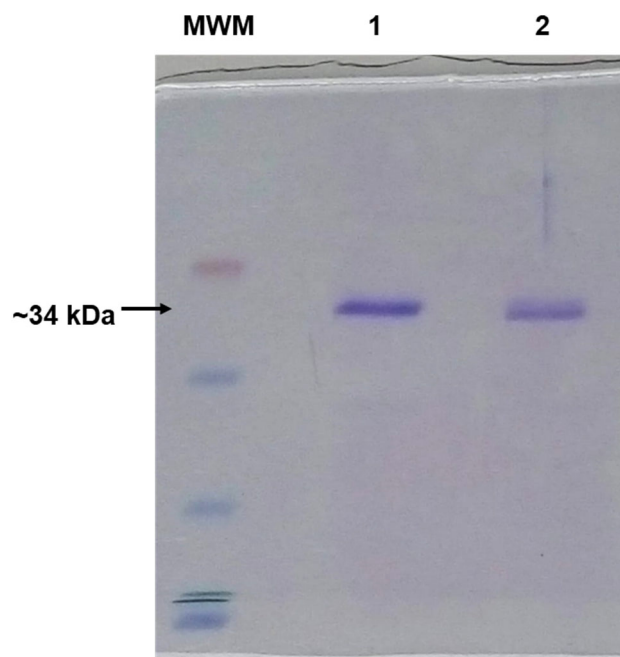


**Figure 8.** SDS-PAGE of human recombinant Cb5R. Lane 1: His<sub>6</sub>-tagged Cb5R. Lane 2: Cb5R after the removal of His<sub>6</sub> by treatment with the Thrombin Clean Cleavage™ kit and passage through a Sephadex G75 column. MWM, lane of molecular weight markers. The gel showed that the treatment with the Thrombin Clean Cleavage™ kit produced the expected decrease of ~1 kDa in the molecular weight and no further proteolytic degradation of Cb5R.

The concentration of recombinant Cb5R was determined using the method of Bradford, with bovine serum albumin as standard or from absorbance measurements at 450 nm, using an extinction coefficient of 11.3 mM<sup>-1</sup>·cm<sup>-1</sup> for the FAD prosthetic group [67,68].

#### 4.4. Preparation of the Human Recombinant Calbindin-D28k and Cb<sub>5</sub>

The human recombinant calbindin-D28k and soluble isoform of Cb<sub>5</sub> have been expressed and purified as described in detail in previous works [40,67,69]. The purified protein were aliquoted and conserved in 30% glycerol at −80 °C until use.

The concentration of recombinant Cb5R was determined using the method of Bradford with bovine serum albumin as standard or from absorbance measurements at 550 nm using a differential extinction coefficient between reduced and oxidized Cb<sub>5</sub> of 16.5 mM<sup>-1</sup>·cm<sup>-1</sup>, as in previous works [67,69].

#### 4.5. Measurements of His<sub>6</sub>, CaM and Calbindin-D28k Interaction with Aβ(1–42) HiLyte™-Fluor555

The change of the fluorescence intensity of Aβ(1–42) HiLyte™-Fluor555 has been used to monitor its complexation with His<sub>6</sub>, CaM and calbindin-D28k. Fluorescence measurements were performed using a Fluoromax+ fluorescence Spectrophotometer (Horiba Jobin Yvon IBH Ltd., Glasgow, UK) in quartz cuvettes of 1cm light pathlength with a total volume of 2.5 mL at room temperature (24–25 °C), with excitation and emission slits of 5 nm.

The measurements of the kinetics of fluorescence have been performed in buffer 50 mM *N*-[2-hydroxyethyl] piperazine-*N'*-[2-ethanesulfonic acid], 100 mM KCl and 50  $\mu$ M CaCl<sub>2</sub> (pH 7.05). The cuvette was kept with magnetic stirring in the dark within the cuvette holder of the fluorimeter until stabilization of the fluorescence intensity after the addition of 10 nM A $\beta$ (1–42) HiLyte™-Fluor555, routinely between 20 and 40 min. Then, His<sub>6</sub> was added to the cuvette at the concentrations indicated in the figures, and the fluorescence intensity was recorded as a function of time with excitation and emission wavelengths of 520 nm and 567 nm, respectively. His<sub>6</sub> was added from stock concentrated solutions prepared in the assay buffer, such that the total added volume was always lower than 10  $\mu$ L. Control experiments were run by adding the same volume of the assay buffer, and showed no significant changes in the fluorescence intensity of A $\beta$ (1–42) HiLyte™-Fluor555.

In the experiments dealing with the effect of His<sub>6</sub> on the kinetics of fluorescence intensity increase after the addition of 5 nM CaM or calbindin-D28k, these proteins were added after 15 min preincubation with the indicated concentration of His<sub>6</sub>. CaM and calbindin-D28k were added from concentrated stock solutions freshly prepared in the assay buffer used in the fluorescence measurements, such that the total added volume was always lower than 10  $\mu$ L.

#### 4.6. *In Silico Docking between A $\beta$ (1–42) and His<sub>6</sub>*

These docking studies have been performed using the MDockPeP Server (<https://zougrouptoolkit.missouri.edu/mdockpep/index.html>), accessed on 26 November 2022. This server generates structural simulations of complexes between proteins and peptides, requiring only the input of the PDB file of the protein and the amino acids sequence of the peptide. In this work, we have used the A $\beta$ (1–42) (PDB: 1IYT) as the protein partner. The server generates the 10 more probable poses for the complex formation, on the basis of the results after three major steps: (1) calculation of peptide conformers, in our case, of His<sub>6</sub>; (2) global flexible sampling of the binding modes protein–peptide; and (3) score and classification of the evaluated types of bonds involved in the formation of the complex [70]. Interacting interfaces were analyzed using PDBePISA [71], access date 4–5 October 2023, and they were visualized using UCSF Chimera [72].

#### 4.7. *Titration with A $\beta$ (1–42) and A $\beta$ (25–35) of the NADH-Dependent Cb<sub>5</sub> Reductase Activity of the Cb5R*

The measurements were performed with a Shimadzu UV1800 spectrophotometer at a wavelength of 550 nm in 1 mL cuvettes containing the assay buffer 20 mM phosphate/0.1 mM diethylenetriaminepentaacetic acid (pH 7), with 0.11  $\mu$ g of Cb5R/mL and 5  $\mu$ M of Cb<sub>5</sub> in the absence and presence of the concentrations of A $\beta$ (1–42), A $\beta$ (25–35) and ‘scrambled’ A $\beta$ (1–42), indicated in the figures. The reaction was started by the addition of 0.25 mM NADH after 10 min preincubation of the Cb5R in the assay medium, and initial rates were measured during periods of time ranging between 5 and 10 min, with a less than 10% drop in the Cb<sub>5</sub> concentration in the assay cuvette. The Cb<sub>5</sub> reductase activity was calculated from the change of absorbance at 550 nm using a differential extinction coefficient between reduced and oxidized Cb<sub>5</sub> of 16.5 mM<sup>-1</sup>·cm<sup>-1</sup>, as in previous works [67,69]. The titration of the NADH-dependent Cb<sub>5</sub> reductase activity of the Cb5R with the A $\beta$  peptide was carried out by measuring in each assay cuvette the activity before and after the addition of each concentration of the A $\beta$  peptide, in order to have an internal control of the activity in the absence of the A $\beta$  peptide to cancel putative minor differences in Cb5R pipetting. The volume of A $\beta$  peptide solution added ranged between 1 and 2.5  $\mu$ L, pipetted from a freshly prepared solution of a prefixed concentration by dilution of aliquots of the stock solution in the assay buffer.

#### 4.8. *Titration with A $\beta$ (1–42) and A $\beta$ (25–35) of the FAD Fluorescence of Human Recombinant Cb5R with a His<sub>6</sub>-Tag and FRET Analysis*

The FAD fluorescence of human recombinant Cb5R with a His<sub>6</sub>-tag (32 nM) has been measured at 25 °C with a Perkin Elmer 650-40 spectrofluorometer in quartz cuvettes of 1 cm

pathlength with excitation and emission wavelengths of 460 nm and 520 nm, respectively, and excitation and emission slits of 10 nm. The assay buffer was 20 mM phosphate/0.1 mM diethylenetriaminepentaacetic acid (pH 7). We noticed that the FAD fluorescence of the recombinant enzyme displays a small but steady increase as a function of time. This indicates a weak instability of the recombinant Cb5R in these experimental conditions because its denaturation produces around a 1000-fold increase in the FAD fluorescence [67]. Due to this, the operational protocol for data acquisition was as follows: after recording the drift of the fluorescence intensity of the Cb5R in the assay buffer for 5 min, A $\beta$  peptides were added at the concentrations indicated in the figures and the fluorescence intensity was recorded for another 5 min. The increase in fluorescence produced by each A $\beta$  peptide concentration shown in the figures was corrected by the drift of fluorescence intensity drift recorded before the addition of the A $\beta$  peptide.

The steady-state anisotropy of fluorescence,  $r_s$ , has been calculated from the polarization of fluorescence (P) using the equation [73]:

$$r_s = 2 \times P / (3 - P). \quad (1)$$

Polarization of fluorescence, P, was calculated using the equation:

$$P = [I_{\parallel} - G \times I_{\perp}] / [I_{\parallel} + G \times I_{\perp}], \quad (2)$$

where  $I_{\parallel}$  and  $I_{\perp}$  are the fluorescence intensities measured with parallel ( $0^\circ/0^\circ$ ) and perpendicularly ( $0^\circ/90^\circ$ ) oriented polarizers, respectively, and G is the correction factor for polarization characteristics of the emission monochromator [62,63,73]. A value of G of  $1.04 \pm 0.02$  has been obtained for our fluorimeter and used in our calculations.

The distance (d) between the Cb5R prosthetic group FAD and the dye HiLyte<sup>TM</sup>-Fluor555 covalently bound to A $\beta$ (1–42), which form a donor–acceptor FRET pair, has been calculated for the cases of 1 and 2 acceptors per donor. In the case of multiple acceptors per donor, the rate constant of total FRET ( $k_T$ ) is the sum of the rate constant of FRET between each donor–acceptor pair ( $k_i$ ) that can be formed in the assembly [74–77]. The total FRET efficiency (E) is the sum of the FRET efficiency for each donor–acceptor pair that is possible with the geometrical constraints of the system [74–76]. For each donor–acceptor pair, we have used the equation for FRET:  $E = d^{-6} / (R_0^{-6} + d^{-6})$  [62]. In this equation, E is the FRET efficiency and  $R_0$  is the distance for 50% FRET efficiency between FAD and HiLyte<sup>TM</sup>-Fluor555. The value of  $R_0$  has been calculated in this work using the operational protocol followed from previous works for other FRET donor–acceptor pairs [61–63]. Briefly, we have applied the equation [62]:

$$R_0 = 9.7 \times 10^3 \times [K^2 \times \Phi_D \times J(\lambda) \times n^{-4}]^{1/6} \times \text{Å} \quad (3)$$

with the assumption of random orientation between donor and acceptor ( $K^2 = 2/3$ ) and the relative refractive index of an aqueous medium ( $n = 1.33$ ). The quantum yield of the donor ( $\Phi_D$ ) and the overlap integral,  $J(\lambda)$ , have been calculated as indicated in Section 2 of this article.

#### 4.9. In Silico Docking Simulation between A $\beta$ (1–42) and Cb5R

Docking between A $\beta$ (1–42) and Cb5R has been performed using the ClusPro server with the following PDB files: A $\beta$ (1–42) (PDB ID: 1IYT) and Cb5R (PDB ID: 1UMK), access date 29 January 2019. The images and analysis of the model structures were built up with the UCSF Chimera software.

#### 4.10. Statistical Analysis

All the results are means  $\pm$  standard error of the mean (S.E.M.) of experiments performed, at least, in triplicate.

**Supplementary Materials:** The following supporting information can be downloaded at: <https://www.mdpi.com/article/10.3390/molecules28207138/s1>, Figure S1: PDB files of the ten most probable model structures generated using the MDockPeP Server for the His<sub>6</sub>/Aβ(1–42) complex; Table S1: Supplementary Table S1; Table S2: Supplementary Table S2; Table S3: Supplementary Table S3.

**Author Contributions:** Conceptualization, C.G.-M. and A.K.S.-A.; methodology, J.S., A.K.S.-A. and C.G.-M.; software, J.S., A.K.S.-A. and C.G.-M.; validation, J.S., A.K.S.-A. and C.G.-M.; formal analysis, J.S. and C.G.-M.; investigation, J.S., A.K.S.-A. and C.G.-M.; resources, C.G.-M.; data curation, J.S. and C.G.-M.; writing—original draft preparation, J.S. and C.G.-M.; writing—review and editing, J.S., A.K.S.-A. and C.G.-M.; supervision, C.G.-M.; project administration, C.G.-M.; funding acquisition, C.G.-M. All authors have read and agreed to the published version of the manuscript.

**Funding:** This work has been supported by Grant BFU2017-85723-P of the Spanish Ministerio de Ciencia, Innovación y Universidades (Spanish National R&D program), which received co-financing by the European Funds for Structural Development (FEDER). Jairo Salazar was supported with a Fellowship of the Spanish Fundación Carolina (Madrid, Spain).

**Institutional Review Board Statement:** Not applicable.

**Informed Consent Statement:** Not applicable.

**Data Availability Statement:** Data supporting the reported results can be found in the laboratory archives of the authors.

**Acknowledgments:** We would like to thank for the support and organization of the Special Issue dedicated to Carlos Gutiérrez-Merino: “Themed Issue in Honor of Carlos Gutiérrez Merino: Forty Years of Research Excellence in the Field of Membrane Proteins and Bioenergetics”.

**Conflicts of Interest:** The authors declare no conflict of interest. The funders had no role in the design of the study; in the collection, analyses, or interpretation of data; in the writing of the manuscript; or in the decision to publish the results.

## Abbreviations

Aβ	amyloid β peptides
AD	Alzheimer’s disease
CaM	calmodulin
Cb <sub>5</sub>	cytochrome <i>b</i> <sub>5</sub>
Cb5R	cytochrome <i>b</i> <sub>5</sub> reductase
ER	endoplasmic reticulum
FAD	flavine adenine dinucleotide
FMN	flavine mononucleotide
FRET	fluorescence resonance energy transfer
His <sub>6</sub>	hexa-histidine
K <sub>d,app</sub>	apparent dissociation constant
K <sub>i</sub>	inhibition constant
SDS-PAGE	sodium dodecyl sulfate polyacrylamide gel electrophoresis
S.E.M.	standard error of the mean

## References

1. Younkin, S.G. The role of Aβ 42 in Alzheimer’s disease. *J. Physiol. Paris* **1998**, *92*, 289–292. [[CrossRef](#)] [[PubMed](#)]
2. Lovell, M.A.; Robertson, J.D.; Teesdale, W.J.; Campbell, J.L.; Markesbery, W.R. Copper, iron and zinc in Alzheimer’s disease senile plaques. *J. Neurol. Sci.* **1998**, *158*, 47–52. [[CrossRef](#)] [[PubMed](#)]
3. Mucke, L.; Selkoe, D.J. Neurotoxicity of Amyloid β-Protein: Synaptic and Network Dysfunction. *Cold Spring Harb. Perspect. Med.* **2012**, *2*, 1–18. [[CrossRef](#)] [[PubMed](#)]
4. Walsh, D.M.; Klyubin, I.; Fadeeva, J.V.; Cullen, W.K.; Anwyl, R.; Wolfe, M.S.; Rowan, M.J.; Selkoe, D.J. Naturally Secreted Oligomers of Amyloid β Protein Potently Inhibit Hippocampal Long-Term Potentiation in Vivo. *Nature* **2002**, *416*, 535–539. [[CrossRef](#)]
5. Gong, Y.; Chang, L.; Viola, K.L.; Lacor, P.N.; Lambert, M.P.; Finch, C.E.; Krafft, G.A.; Klein, W.L. Alzheimer’s Disease-Affected Brain: Presence of Oligomeric Aβ Ligands (ADDLs) Suggests a Molecular Basis for Reversible Memory Loss. *Proc. Natl. Acad. Sci. USA* **2003**, *100*, 10417–10422. [[CrossRef](#)]

6. Knobloch, M.; Konietzko, U.; Krebs, D.C.; Nitsch, R.M. Intracellular A $\beta$  and cognitive deficits precede  $\beta$ -amyloid deposition in transgenic arcA $\beta$  mice. *Neurobiol. Aging* **2007**, *28*, 1297–1306. [[CrossRef](#)]
7. Shankar, G.M.; Li, S.; Mehta, T.H.; Garcia-Munoz, A.; Shepardson, N.E.; Smith, I.; Brett, F.M.; Farrell, M.A.; Rowan, M.J.; Lemere, C.A.; et al. Amyloid  $\beta$ -Protein Dimers Isolated Directly from Alzheimer Brains Impair Synaptic Plasticity and Memory. *Nat. Med.* **2008**, *14*, 837–842. [[CrossRef](#)]
8. Hu, X.; Crick, S.L.; Bu, G.; Frieden, C.; Pappu, R.V.; Lee, J.-M. Amyloid seeds formed by cellular uptake, concentration, and aggregation of the amyloid- $\beta$  peptide. *Proc. Natl. Acad. Sci. USA* **2009**, *106*, 20324–20329. [[CrossRef](#)] [[PubMed](#)]
9. Friedrich, R.P.; Tepper, K.; Rönicke, R.; Soom, M.; Westermann, M.; Reymann, K.; Kaether, C.; Fändrich, M. Mechanism of amyloid plaque formation suggests an intracellular basis of A $\beta$  pathogenicity. *Proc. Natl. Acad. Sci. USA* **2010**, *107*, 1942–1947. [[CrossRef](#)]
10. He, Y.; Zheng, M.M.; Ma, Y.; Han, X.J.; Ma, X.Q.; Qu, C.Q.; Du, Y.F. Soluble Oligomers and Fibrillar Species of Amyloid  $\beta$ -Peptide Differentially Affect Cognitive Functions and Hippocampal Inflammatory Response. *Biochem. Biophys. Res. Commun.* **2012**, *429*, 125–130. [[CrossRef](#)]
11. Forny-Germano, L.; Lyra e Silva, N.M.; Batista, A.F.; Brito-Moreira, J.; Gralle, M.; Boehnke, S.E.; Coe, B.C.; Lablans, A.; Marques, S.A.; Martinez, A.M.; et al. Alzheimer's Disease-like Pathology Induced by Amyloid- $\beta$  Oligomers in Nonhuman Primates. *J. Neurosci.* **2014**, *34*, 13629–13643. [[CrossRef](#)] [[PubMed](#)]
12. Wirths, O.; Multhaup, G.; Czech, C.; Blanchard, V.; Moussaoui, S.; Tremp, G.; Pradier, L.; Beyreuther, K.; Bayer, T.A. Intraneuronal A $\beta$  accumulation precedes plaque formation in  $\beta$ -amyloid precursor protein and presenilin-1 double-transgenic mice. *Neurosci. Lett.* **2001**, *306*, 116–120. [[CrossRef](#)] [[PubMed](#)]
13. Oddo, S.; Caccamo, A.; Shephard, J.D.; Murphy, M.P.; Golde, T.E.; Kaye, R.; Metherate, R.; Mattson, M.P.; Akbari, Y.; LaFerla, F.M. Triple-transgenic model of Alzheimer's disease with plaques and tangles: Intracellular A $\beta$  and synaptic dysfunction. *Neuron* **2003**, *39*, 409–421. [[CrossRef](#)] [[PubMed](#)]
14. Oakley, H.; Cole, S.L.; Logan, S.; Maus, E.; Shao, P.; Craft, J.; Guillozet-Bongaarts, A.; Ohno, M.; Disterhoft, J.; Van Eldik, L.; et al. Intraneuronal  $\beta$ -amyloid aggregates, neurodegeneration, and neuron loss in transgenic mice with five familial Alzheimer's disease mutations: Potential factors in amyloid plaque formation. *J. Neurosci.* **2006**, *26*, 10129–10140. [[CrossRef](#)]
15. Millucci, L.; Ghezzi, L.; Bernardini, G.; Santucci, A. Conformations and biological activities of amyloid beta peptide 25–35. *Curr. Protein Pept. Sci.* **2010**, *11*, 54–67. [[CrossRef](#)] [[PubMed](#)]
16. Pike, C.J.; Walencewicz-Wasserman, A.J.; Kosmoski, J.; Cribbs, D.H.; Glabe, C.G.; Cotman, C.W. Structure-activity analyses of beta-amyloid peptides: Contributions of the beta 25–35 region to aggregation and neurotoxicity. *J. Neurochem.* **1995**, *64*, 253–265. [[CrossRef](#)] [[PubMed](#)]
17. Frozza, R.L.; Horn, A.P.; Hoppe, J.B.; Simão, F.; Gerhardt, D.; Comiran, R.A.; Salbego, C.G. A comparative study of beta-amyloid peptides Abeta1–42 and Abeta25–35 toxicity in organotypic hippocampal slice cultures. *Neurochem. Res.* **2009**, *34*, 295–303. [[CrossRef](#)] [[PubMed](#)]
18. Choo-Smith, L.P.; Garzon-Rodriguez, W.; Glabe, C.G.; Surewicz, W.K. Acceleration of amyloid fibril formation by specific binding of A $\beta$ -(1–40) peptide to ganglioside containing membrane vesicles. *J. Biol. Chem.* **1997**, *272*, 22987–22990. [[CrossRef](#)]
19. Kakio, A.; Nishimoto, S.I.; Yanagisawa, K.; Kozutsumi, Y.; Matsuzaki, K. Cholesterol dependent formation of GM1 ganglioside-bound amyloid  $\beta$ -protein, an endogenous seed for Alzheimer amyloid. *J. Biol. Chem.* **2001**, *276*, 24985–24990. [[CrossRef](#)] [[PubMed](#)]
20. Kakio, A.; Nishimoto, S.; Yanagisawa, K.; Kozutsumi, Y.; Matsuzaki, K. Interactions of amyloid  $\beta$ -protein with various gangliosides in raft-like membranes: Importance of GM1 ganglioside-bound form as an endogenous seed for Alzheimer amyloid. *Biochemistry* **2002**, *41*, 7385–7390. [[CrossRef](#)]
21. Wood, W.G.; Schroeder, F.; Igbavboa, U.; Avdulov, N.A.; Chochina, S.V. Brain membrane cholesterol domains, aging and amyloid beta-peptides. *Neurobiol. Aging* **2002**, *23*, 685–694. [[CrossRef](#)] [[PubMed](#)]
22. Matsuzaki, K.; Kato, K.; Yanagisawa, K. A $\beta$  polymerization through interaction with membrane gangliosides. *Biochim. Biophys. Acta* **2010**, *1801*, 868–877. [[CrossRef](#)] [[PubMed](#)]
23. Kawarabayashi, T.; Shoji, M.; Younkin, L.H.; Wen-Lang, L.; Dickson, D.W.; Murakami, T.; Matsubara, E.; Abe, K.; Ashe, K.H.; Younkin, S.G. Dimeric amyloid beta protein rapidly accumulates in lipid rafts followed by apolipoprotein E and phosphorylated tau accumulation in the Tg2576 mouse model of Alzheimer's disease. *J. Neurosci.* **2004**, *24*, 3801–3809. [[CrossRef](#)] [[PubMed](#)]
24. Williamson, R.; Usardi, A.; Hanger, D.P.; Anderton, B.H. Membrane-bound beta-amyloid oligomers are recruited into lipid rafts by a fyn-dependent mechanism. *FASEB J.* **2008**, *22*, 1552–1559. [[CrossRef](#)] [[PubMed](#)]
25. Lai, A.Y.; McLaurin, J.A. Mechanisms of Amyloid-Beta Peptide Uptake by Neurons: The Role of Lipid Rafts and Lipid Raft-Associated Proteins. *Int. J. Alzheimer's Dis.* **2011**, *2011*, 548380. [[CrossRef](#)]
26. Jin, S.; Kedia, N.; Illes-Toth, E.; Haralampiev, I.; Prisner, S.; Herrmann, A.; Wanker, E.E.; Bieschke, J. Amyloid- $\beta$ (1–42) Aggregation Initiates Its Cellular Uptake and Cytotoxicity. *J. Biol. Chem.* **2016**, *291*, 19590–19606. [[CrossRef](#)]
27. Poejo, J.; Salazar, J.; Mata, A.M.; Gutierrez-Merino, C. Binding of Amyloid  $\beta$ (1–42)-Calmodulin Complexes to Plasma Membrane Lipid Rafts in Cerebellar Granule Neurons Alters Resting Cytosolic Calcium Homeostasis. *Int. J. Mol. Sci.* **2021**, *22*, 1984. [[CrossRef](#)]
28. Umeda, T.; Tomiyama, T.; Sakama, N.; Tanaka, S.; Lambert, M.P.; Klein, W.L.; Mori, H. Intraneuronal Amyloid  $\beta$  Oligomers Cause Cell Death Via Endoplasmic Reticulum Stress, Endosomal/Lysosomal Leakage, and Mitochondrial Dysfunction In Vivo. *J. Neurosci. Res.* **2011**, *89*, 1031–1042. [[CrossRef](#)]

29. Cha, M.Y.; Han, S.H.; Son, S.M.; Hong, H.-S.; Choi, Y.-J.; Byun, J.; Mook-Jung, I. Mitochondria-Specific Accumulation of Amyloid  $\beta$  Induces Mitochondrial Dysfunction Leading to Apoptotic Cell Death. *PLoS ONE* **2012**, *7*, e34929. [[CrossRef](#)]
30. Poejo, J.; Orantos-Aguilera, Y.; Martin-Romero, F.J.; Mata, A.M.; Gutierrez-Merino, C. Internalized Amyloid- $\beta$  (1-42) Peptide Inhibits the Store-Operated Calcium Entry in HT-22 Cells. *Int. J. Mol. Sci.* **2022**, *23*, 12678. [[CrossRef](#)]
31. Podlisny, M.B.; Walsh, D.M.; Amarante, P.; Ostaszewski, B.L.; Stimson, E.R.; Maggio, J.E.; Teplow, D.B.; Selkoe, D.J. Oligomerization of endogenous and synthetic amyloid  $\beta$ -protein at nanomolar levels in cell culture and stabilization of monomer by Congo red. *Biochemistry* **1998**, *37*, 3602–3611. [[CrossRef](#)]
32. Selkoe, D.J. Alzheimer's disease: Genes, proteins, and therapy. *Physiol. Rev.* **2001**, *81*, 741–766. [[CrossRef](#)]
33. Cleary, J.P.; Walsh, D.M.; Hofmeister, J.J.; Shankar, G.M.; Kuskowski, M.A.; Selkoe, D.J.; Ashe, K.H. Natural oligomers of the amyloid- $\beta$  protein specifically disrupt cognitive function. *Nat. Neurosci.* **2005**, *8*, 79–84. [[CrossRef](#)] [[PubMed](#)]
34. Hellstrand, E.; Boland, B.; Walsh, D.M.; Linse, S. Amyloid  $\beta$ -protein aggregation produces highly reproducible kinetic data and occurs by a two-phase process. *ACS Chem. Neurosci.* **2009**, *1*, 13–18. [[CrossRef](#)] [[PubMed](#)]
35. Hamley, I.W. The amyloid beta peptide: A chemist's perspective. Role in Alzheimer's and fibrillization. *Chem. Rev.* **2012**, *112*, 5147–5192. [[CrossRef](#)] [[PubMed](#)]
36. Corbacho, I.; Berrocal, M.; Török, K.; Mata, A.M.; Gutierrez-Merino, C. High affinity binding of amyloid  $\beta$ -peptide to calmodulin: Structural and functional implications. *Biochem. Biophys. Res. Commun.* **2017**, *486*, 992–997. [[CrossRef](#)]
37. Laurén, J.; Gimbel, D.A.; Nygaard, H.B.; Gilbert, J.W.; Strittmatter, S.M. Cellular prion protein mediates impairment of synaptic plasticity by amyloid- $\beta$  oligomers. *Nat. Cell Biol.* **2009**, *457*, 1128–1132. [[CrossRef](#)]
38. Dunning, C.J.; McGauran, G.; Willén, K.; Gouras, G.K.; O'Connell, D.J.; Linse, S. Direct High Affinity Interaction between A $\beta$ 42 and GSK3 $\alpha$  Stimulates Hyperphosphorylation of Tau. A New Molecular Link in Alzheimer's Disease? *ACS Chem. Neurosci.* **2015**, *7*, 161–170. [[CrossRef](#)]
39. Guo, J.-P.; Arai, T.; Miklossy, J.; McGeer, P.L. A $\beta$  and tau form soluble complexes that may promote self-aggregation of both into the insoluble forms observed in Alzheimer's disease. *Proc. Natl. Acad. Sci. USA* **2006**, *103*, 1953–1958. [[CrossRef](#)]
40. Salazar, J.; Poejo, J.; Mata, A.M.; Samhan-Arias, A.K.; Gutierrez-Merino, C. Design and Experimental Evaluation of a Peptide Antagonist against Amyloid  $\beta$ (1-42) Interactions with Calmodulin and Calbindin-D28k. *Int. J. Mol. Sci.* **2022**, *23*, 2289. [[CrossRef](#)]
41. Baimbridge, K.G.; Celio, M.R.; Rogers, J.H. Calcium-binding proteins in the nervous system. *Trends Neurosci.* **1992**, *15*, 303–308. [[CrossRef](#)]
42. Kuchibhotla, K.V.; Goldman, S.T.; Lattarulo, C.R.; Wu, H.Y.; Hyman, B.T.; Bacskai, B.J. A $\beta$  Plaques Lead to Aberrant Regulation of Calcium Homeostasis in Vivo Resulting in Structural and Functional Disruption of Neuronal Networks. *Neuron* **2008**, *59*, 214–225. [[CrossRef](#)] [[PubMed](#)]
43. Lopez, R.; Lyckman, A.; Oddo, S.; Laferla, F.M.; Querfurth, H.W.; Shtifman, A. Increased Intraneuronal Resting [Ca<sup>2+</sup>] in Adult Alzheimer's Disease Mice. *J. Neurochem.* **2008**, *105*, 262–271. [[CrossRef](#)] [[PubMed](#)]
44. Berridge, M.J. Calcium Signalling and Alzheimer's Disease. *Neurochem. Res.* **2011**, *36*, 1149–1156. [[CrossRef](#)] [[PubMed](#)]
45. Poejo, J.; Salazar, J.; Mata, A.M.; Gutierrez-Merino, C. The Relevance of Amyloid  $\beta$ -Calmodulin Complexation in Neurons and Brain Degeneration in Alzheimer's Disease. *Int. J. Mol. Sci.* **2021**, *22*, 4976. [[CrossRef](#)]
46. dos Santos, V.V.; Santos, D.B.; Lach, G.; Rodrigues, A.L.; Farina, M.; De Lima, T.C.; Prediger, R.D. Neuropeptide Y (NPY) prevents depressive-like behavior, spatial memory deficits and oxidative stress following amyloid- $\beta$  [A $\beta$ (1-40)] administration in mice. *Behav. Brain Res.* **2013**, *244*, 107–115. [[CrossRef](#)]
47. Kang, S.; Moon, N.R.; Kim, D.S.; Kim, S.H.; Park, S. Central acylated ghrelin improves memory function and hippocampal AMPK activation and partly reverses the impairment of energy and glucose metabolism in rats infused with  $\beta$ -amyloid. *Peptides* **2015**, *71*, 84–93. [[CrossRef](#)]
48. Santos, V.V.; Stark, R.; Rial, D.; Silva, H.B.; Bayliss, J.A.; Lemus, M.B.; J S Davies, J.S.; Cunha, R.A.; Prediger, R.D.; Andrews, Z.B. Acyl ghrelin improves cognition, synaptic plasticity deficits and neuroinflammation following amyloid  $\beta$  (A $\beta$ 1-40) administration in mice. *J. Neuroendocrinol.* **2017**, *29*, 1–11. [[CrossRef](#)] [[PubMed](#)]
49. Martins, I.; Gomes, S.; Costa, R.O.; Otvos, L.; Oliveira, C.R.; Resende, R.; Pereira, C.M.F. Leptin and ghrelin prevent hippocampal dysfunction induced by A $\beta$  oligomers. *Neuroscience* **2013**, *241*, 41–51. [[CrossRef](#)]
50. Gomes, S.; Martins, I.; Fonseca, A.C.; Oliveira, C.R.; Resende, R.; Pereira, C.M. Protective effect of leptin and ghrelin against toxicity induced by amyloid- $\beta$  oligomers in a hypothalamic cell line. *J. Neuroendocrinol.* **2014**, *26*, 176–185. [[CrossRef](#)]
51. Poon, I.K.; Patel, K.K.; Davis, D.S.; Parish, C.R.; Hulett, M.D. Histidine-rich glycoprotein: The Swiss Army knife of mammalian plasma. *Blood* **2011**, *117*, 2093–2101. [[CrossRef](#)]
52. Potocki, S.; Valensinb, D.; Kozlowski, H. The specificity of interaction of Zn<sup>2+</sup>, Ni<sup>2+</sup> and Cu<sup>2+</sup> ions with the histidine-rich domain of the TjZNT1 ZIP family transporter. *Dalton Trans.* **2014**, *43*, 10215–10223. [[CrossRef](#)] [[PubMed](#)]
53. Priebatsch, K.M.; Kvensakul, M.; Poon, I.K.; Hulett, M.D. Functional Regulation of the Plasma Protein Histidine-Rich Glycoprotein by Zn<sup>2+</sup> in Settings of Tissue Injury. *Biomolecules* **2017**, *7*, 22. [[CrossRef](#)] [[PubMed](#)]
54. Atwood, C.S.; Scarpa, R.C.; Huang, X.; Moir, R.D.; Jones, W.D.; Fairlie, D.P.; Tanzi, R.E.; Bush, A.I. Characterization of copper interactions with alzheimer amyloid beta peptides: Identification of an attomolar-affinity copper binding site on amyloid beta1-42. *J. Neurochem.* **2000**, *75*, 1219–1233. [[CrossRef](#)] [[PubMed](#)]
55. Teplyakov, A.; Obmolova, G.; Canziani, G.; Zhao, Y.; Gutshall, L.; Jung, S.S.; Gilliland, G.L. His-tag binding by antibody C706 mimics  $\beta$ -amyloid recognition. *J. Mol. Recognit.* **2011**, *24*, 570–575. [[CrossRef](#)] [[PubMed](#)]

56. Rojo, L.; Sjöberg, M.K.; Hernández, P.; Zambrano, C.; Maccioni, R.B. Roles of cholesterol and lipids in the etiopathogenesis of Alzheimer's disease. *BioMed Res. Int.* **2006**, *2006*, 073976. [[CrossRef](#)]
57. Lee, H.J.; Korshavn, K.J.; Kochi, A.; Derrick, J.S.; Lim, M.H. Cholesterol and metal ions in Alzheimer's disease. *Chem. Soc. Rev.* **2014**, *43*, 6672–6682. [[CrossRef](#)]
58. Andreetto, E.; Yan, L.M.; Tatarek-Nossol, M.; Velkova, A.; Frank, R.; Kapurniotu, A. Identification of Hot Regions of the A $\beta$ -IAPP Interaction Interface as High-Affinity Binding Sites in both Cross- and Self-Association. *Angew. Chem. Int. Ed.* **2010**, *49*, 3081–3085. [[CrossRef](#)]
59. Samhan-Arias, A.K.; Maia, L.B.; Cordas, C.M.; Moura, I.; Gutierrez-Merino, C.; Moura, J. Peroxidase-like activity of cytochrome *b*<sub>5</sub> is triggered upon hemichrome formation in alkaline pH. *Biochim. Biophys. Acta BBA-Proteins Proteom.* **2018**, *1866*, 373–378. [[CrossRef](#)]
60. Samhan-Arias, A.K.; Cordas, C.M.; Carepo, M.S.; Maia, L.B.; Gutierrez-Merino, C.; Moura, I.; Moura, J. Ligand accessibility to heme cytochrome *b*<sub>5</sub> coordinating sphere and enzymatic activity enhancement upon tyrosine ionization. *J. Biol. Inorg. Chem.* **2019**, *24*, 317–330. [[CrossRef](#)] [[PubMed](#)]
61. Gutierrez-Merino, C.; Molina, A.; Escudero, B.; Diez, A.; Laynez, J. Interaction of the Local Anesthetics Dibucaine and Tetracaine with Sarcoplasmic Reticulum Membranes. Differential Scanning Calorimetry and Fluorescence Studies. *Biochemistry* **1989**, *28*, 3398–3406. [[CrossRef](#)]
62. Centeno, F.; Gutierrez-Merino, C. Location of Functional Centers in the Microsomal Cytochrome P450 System. *Biochemistry* **1992**, *31*, 8473–8481. [[CrossRef](#)] [[PubMed](#)]
63. Tiago, T.; Aureliano, M.; Gutiérrez-Merino, C. Decavanadate binding to a high affinity site near the myosin catalytic centre inhibits F-actin-stimulated myosin ATPase activity. *Biochemistry* **2004**, *43*, 5551–5561. [[CrossRef](#)] [[PubMed](#)]
64. Riguero, V.; Clifford, R.; Dawley, M.; Dickson, M.; Gastfriend, B.; Thompson, C.; Wang, S.C.; O'Connor, E. Immobilized metal affinity chromatography optimization for poly-histidine tagged proteins. *J. Chromatogr. A* **2020**, *1629*, 461505. [[CrossRef](#)] [[PubMed](#)]
65. Stryer, L. Fluorescence Energy Transfer as a Spectroscopic Ruler. *Annu. Rev. Biochem.* **1978**, *47*, 819–846. [[CrossRef](#)] [[PubMed](#)]
66. Gutiérrez-Merino, C.; Martínez-Costa, O.H.; Monsalve, M.; Samhan-Arias, A.K. Structural Features of Cytochrome *b*<sub>5</sub>-Cytochrome *b*<sub>5</sub> Reductase Complex Formation and Implications for the Intramolecular Dynamics of Cytochrome *b*<sub>5</sub> Reductase. *Int. J. Mol. Sci.* **2022**, *23*, 118. [[CrossRef](#)] [[PubMed](#)]
67. Samhan-Arias, A.K.; Almeida, R.M.; Ramos, S.; Cordas, C.M.; Moura, I.; Gutierrez-Merino, C.; Moura, J. Topography of human cytochrome *b*<sub>5</sub>/cytochrome *b*<sub>5</sub> reductase interacting domain and redox alterations upon complex formation. *Biochim. Biophys. Acta BBA-Proteins Proteom.* **2018**, *1859*, 78–87. [[CrossRef](#)]
68. van den Berg, P.A.; Widengren, J.; Hink, M.A.; Rigler, R.; Visser, A.J. Fluorescence correlation spectroscopy of flavins and flavoenzymes: Photochemical and photophysical aspects. *Spectrochim. Acta. Part A Mol. Biomol. Spectrosc.* **2001**, *57*, 2135–2144. [[CrossRef](#)]
69. Gómez-Tabales, J.; García-Martín, E.; Agúndez, J.; Gutierrez-Merino, C. Modulation of CYP2C9 activity and hydrogen peroxide production by cytochrome *b*<sub>5</sub>. *Sci. Rep.* **2020**, *10*, 15571. [[CrossRef](#)]
70. Xu, X.; Yan, C.; Zou, X. MDockPeP: An ab-initio protein-peptide docking server. *J. Comput. Chem.* **2018**, *39*, 2409–2413. [[CrossRef](#)]
71. Krissinel, E.; Henrick, K. Inference of macromolecular assemblies from crystalline state. *J. Mol. Biol.* **2007**, *372*, 774–797. [[CrossRef](#)] [[PubMed](#)]
72. Pettersen, E.F.; Goddard, T.D.; Huang, C.C.; Couch, G.S.; Greenblatt, D.M.; Meng, E.C.; Ferrin, T.E. UCSF Chimera—a visualization system for exploratory research and analysis. *J. Comput. Chem.* **2004**, *25*, 1605–1612. [[CrossRef](#)] [[PubMed](#)]
73. Lakowicz, J.R. *Principles of Fluorescence Spectroscopy*, 3rd ed.; Springer: New York, NY, USA, 2010; ISBN 978-0-387-31278-1.
74. Gutiérrez-Merino, C. Quantitation of the Forster Energy Transfer for Bidimensional Systems: I) Lateral Phase Separation in Unilamellar Vesicles Formed by Binary Phospholipid Mixtures. *Biophys. Chem.* **1981**, *14*, 247–257. [[CrossRef](#)]
75. Gutiérrez-Merino, C. Quantitation of the Forster Energy Transfer for Bidimensional Systems: II) Protein Distribution and Aggregation State in Biological Membranes. *Biophys. Chem.* **1981**, *14*, 259–266. [[CrossRef](#)] [[PubMed](#)]
76. Gutiérrez-Merino, C.; Centeno, F.; García Martín, E.; Merino, J.M. Fluorescence energy transfer as a tool to locate functional sites in membrane proteins. *Biochem. Soc. Trans.* **1994**, *22*, 784–788. [[CrossRef](#)] [[PubMed](#)]
77. Gutiérrez-Merino, C.; Bonini de Romanelli, I.C.; Pietrasanta, L.I.; Barrantes, F.J. Preferential distribution of the fluorescent phospholipid probes NBD phosphatidylcholine and rhodamine phosphatidylethanolamine in the exofacial leaflet of acetylcholine receptor rich membranes from *Torpedo marmorata*. *Biochemistry* **1995**, *34*, 4846–4855. [[CrossRef](#)] [[PubMed](#)]

**Disclaimer/Publisher's Note:** The statements, opinions and data contained in all publications are solely those of the individual author(s) and contributor(s) and not of MDPI and/or the editor(s). MDPI and/or the editor(s) disclaim responsibility for any injury to people or property resulting from any ideas, methods, instructions or products referred to in the content.